Immunoproximity biotinylation reveals the axon initial segment proteome

Wei Zhang[1,2,3], Yu Fu[1], Luxin Peng[1], Yuki Ogawa[3], Xiaoyun Ding[3], Anne Rasband[3], Xinyue Zhou[2], Maya Shelly[5], Matthew N. Rasband[3*], Peng Zou[1,2,4*]

1. College of Chemistry and Molecular Engineering, Synthetic and Functional Biomolecules Center, Beijing National Laboratory for Molecular Sciences, PKU-IDG/McGovern Institute for Brain Research, Key Laboratory of Bioorganic Chemistry and Molecular Engineering of Ministry of Education, Peking University, Beijing, 100871, China
2. Academy for Advanced Interdisciplinary Studies, PKU-Tsinghua Center for Life Science, Peking University, Beijing 100871, China
3. Department of Neuroscience, Baylor College of Medicine, Houston, TX, USA
4. Chinese Institute for Brain Research (CIBR), Beijing 102206, China
5. Department of Neurobiology and Behavior, Stony Brook University, NY, USA

[*] Correspondence: zoupeng@pku.edu.cn (P.Z.); rasband@bcm.edu (M.N.R)

ABSTRACT

The axon initial segment (AIS) is a specialized neuronal compartment required for action potential generation and neuronal polarity. However, understanding the mechanisms regulating AIS structure and function has been hindered by an incomplete knowledge of its molecular composition. Here, using immuno-proximity biotinylation we further define the AIS proteome and its dynamic changes during neuronal maturation. Among the many AIS proteins identified, we show that SCRIB is highly enriched in the AIS both *in vitro* and *in vivo,* and exhibits a periodic architecture like the axonal spectrin-based cytoskeleton. We found that ankyrinG interacts with and recruits SCRIB to the AIS. However, loss of SCRIB has no effect on ankyrinG. This powerful and flexible approach further defines the AIS proteome and provides a rich resource to elucidate the mechanisms regulating AIS structure and function.

KEYWORDS

axon initial segment, proteomics, proximity labeling, SCRIB, ankyrinG, neuron

INTRODUCTION

The axon initial segment (AIS) is the 20~60 µm long proximal region of the axon responsible for action potential generation and maintenance of neuronal polarity [1, 2]. Changes in the molecular composition of the AIS, its length, or position can alter neuronal excitability [3, 4, 5]. Disruption of the AIS causes axons to acquire dendritic characteristics [6, 7]. Recent studies show that AIS disruption occurs in many neurological diseases including autism, Alzheimer's disease, stroke, bipolar disorder and schizophrenia [8]. Rescuing AIS integrity and function can ameliorate neurological symptoms in Alzheimer's disease and Angelman Syndrome mouse models [9, 10]. However, our incomplete knowledge of AIS components hinders our understanding of the structural and functional regulation of AIS in health and disease.

Axon initial segments consist of a specialized extracellular matrix, clustered cell adhesion molecules (CAMs) and voltage gated ion channels, and a unique cytoskeleton. Among the previously reported AIS proteins, the scaffolding protein ankyrinG (AnkG) is the master organizer for AIS assembly and maintenance [8]. AnkG links membrane proteins to the actin cytoskeleton through a tetramer consisting of βIV and αII-spectrin, and to the microtubule cytoskeleton through the end binding proteins EB1 and EB3 [11]. At the AIS, microtubules form parallel fascicles thought to be organized by TRIM46 [12, 13]. As the site for axonal action potential initiation, AIS also have voltage gated sodium (e.g. Nav1.2), potassium (e.g. Kv7) and calcium channels (e.g. Cav2) that regulate spike generation, pattern and shape [14]. NF186, a neuron-specific isoform of the CAM neurofascin (NFASC), assembles and links extracellular matrix molecules (e.g. Brevican) to the AIS cytoskeleton [15]. In addition, some synaptic proteins (e.g. Gephyrin), cisternal organelle molecules (e.g. Synaptopodin) and a Kv1 channel complex can also be found at the AIS [16].

The combination of enzyme-mediated proximity-dependent biotinylation and mass spectrometry-based quantitative proteomics has emerged as a powerful tool to elucidate endogenous protein complexes in subcellular domains. Two main categories of proximity

62 labeling methods have been developed based on enzymes used for catalysis: biotin ligase-
63 based proximity labeling (e.g. BioID and TurboID) and peroxidase-based proximity
64 labeling (e.g. HRP and APEX2). Pioneering experiments using AIS-targeted BioID were
65 recently used to uncover a partial AIS proteome. However, the experiments were
66 restricted to cytoplasmic AIS proteins and the labeling radius of BioID is confined to ~10
67 nm [17].

68 Here, we report the development of **i**mmuno **p**roximity **l**abeling in fixed neurons,
69 together with a multiple ratiometric analysis strategy to define the **AIS** proteome (IPL-
70 AIS). This method targets endogenous baits without requiring genetic manipulation, thus
71 avoiding potential artifacts from over-expression or fusion proteins with altered
72 subcellular localization [18, 19, 20]. This approach also has the advantage of a larger labeling
73 radius by peroxidase-mediated protein biotinylation in permeabilized and fixed samples
74 [21], allowing us to deeply mine AIS structural components. We applied quantitative
75 ratiometric proteomics with multiple controls to identify AIS proteins [22, 23], allowing us to
76 compare the relative expression of proteins in the AIS against other neuronal
77 compartments (axon, dendrites or soma).

78 IPL-AIS profiling at days *in vitro* (DIV) 7, 14 and 21 revealed the dynamic changes in
79 AIS components during neuronal development. Subsequent validation confirmed the
80 identification of novel AIS enriched proteins, including the tumor-suppressor protein
81 scribble (SCRIB encoded by the gene *Scrib*). We found that SCRIB is highly enriched in the
82 AIS *in vitro* and *in vivo*. In addition, AnkG interacts with SCRIB and is required for SCRIB
83 localization to the AIS. Together, our experiments define the AIS proteome, which paves
84 the way to understand the molecular mechanisms regulating AIS structure and function.
85

86 **RESULTS**

87 **Development of antibody targeted proximity labeling at the AIS**

88 The CAM NF186 is highly and stably localized in the AIS [24, 25], therefore we used
89 NF186 for antibody targeted proximity labeling at the AIS. As illustrated in Fig. 1a, cultured
90 cortical neurons were fixed and labeled using antibodies to restrict horseradish peroxidase
91 (HRP) to the AIS. HRP-mediated proximity-dependent biotinylation is triggered with the
92 addition of biotin-phenol substrates and hydrogen peroxide. Biotinylation can be
93 evaluated with fluorescent streptavidin and immunoblot analysis. Following enrichment
94 via affinity purification, biotinylated proteins are digested with trypsin and identified via
95 quantitative LC-MS/MS analysis.

96 We optimized antibody dilutions, H_2O_2 concentration, reaction time and different
97 biotin-phenol (BP) and biotin- aniline (BA) probes in the proximity labeling system using
98 mature fixed cortical neurons (Supplementary Fig. 1). We found that with optimized
99 conditions we could achieve robust labeling and specificity after just one minute. Previous
100 studies showed the peroxidase substrate BP2 performs well for labeling of cytosolic
101 protein complexes [26], while the substrates BA1 and BA2 exhibit higher reactivity towards
102 nucleic acids (Supplementary Fig. 1e) [27]. Our analysis revealed biotin-phenol (BP) as the
103 most efficient and specific substrate for *in vitro* AIS proximity labeling. We employed these
104 optimized parameters and found strongly biotinylated proteins localized in the AIS (Fig.
105 1b). Through imaging, we also tested other AIS-directed antibodies for proximity labeling,
106 including antibodies against AnkG and TRIM46. In our hands, NFASC targeted proximity
107 labeling exhibited the best performance, with less background and highly specific
108 biotinylation of AIS.

109 To remove background signal arising from non-specific binding of antibodies,
110 experiments omitting the primary antibody (i.e. anti-NFASC) were used as the negative
111 control. To quantify the level of protein enrichment at the AIS, we used NeuN and MAP2
112 to define soma and somatodendritic domains, respectively. NeuN localizes in the nuclei
113 and cytoplasm of neurons [28, 29], while MAP2 is a microtubule-associated protein that is
114 widely distributed throughout the soma and dendrites [5, 30]. Fluorescence microscopy

115 showed highly colocalized biotinylation and immunofluorescence labeling for both NeuN
116 and MAP2 (Fig. 1b). Thus, we applied the same experimental workflow to anti-NeuN and
117 anti-MAP2 defined compartments and used these as references for ratiometric analysis
118 of the AIS proteome.

119 Biochemical characterization by streptavidin-HRP blot and silver staining showed
120 successful protein biotinylation from anti-NFASC, anti-NeuN, and anti-MAP2 proximity
121 labeling experiments (Fig. 1c). As expected, the negative control sample omitting primary
122 antibody yielded significantly less signal; any background signal presumably arose from
123 detection of endogenously biotinylated proteins. Notably, the biotinylation signal was
124 stronger in anti-NeuN and anti-MAP2 reference samples compared to the anti-NFASC
125 sample, which may reflect the higher abundance of and larger volume occupied by NeuN
126 and MAP2.

127 To quantitatively compare protein abundance between samples, we designed the
128 following sets of dimethyl labeling-based ratiometric MS proteomic experiments: 1) anti-
129 NFASC vs. no primary antibody; 2) anti-NFASC vs. anti-NeuN; and 3) anti-NFASC vs. anti-
130 MAP2. The first experiment served to remove background labeling arising from non-
131 specific staining of secondary antibody-HRP conjugates, endogenous biotinylated proteins,
132 and non-specific protein adsorption on streptavidin-coated beads. The next two
133 experiments allowed distinction of AIS-specific proteins from those broadly distributed
134 across the cell. For each set of experiments, three biological replicates were performed
135 on cultured cortical neurons at DIV14 (Fig. 1d).

136 A total of 568 proteins were identified after a stringent cut-off analysis (see Methods),
137 among which several known AIS proteins, including TRIM46, AnkG, and NFASC were highly
138 enriched in our dataset (Fig. 1e and Supplementary Table 1). On the other hand, we
139 noticed the low enrichment of EB1 and SEPTIN5, which are also found at the AIS, but not
140 restricted to the AIS [11, 17], which explains their lack of specific enrichment in our

experiments. Taken together, these results demonstrate that the AIS proteome can be defined using our IPL-AIS methods.

Identification of AIS proteome at DIV14

Building upon the success of our pilot IPL-AIS experiments, we next sought to improve the quality of our proteomic dataset through implementing the following changes in the workflow (Fig. 2a, b): 1) to improve protein abundance quantitation across multiple samples, we introduced Tandem Mass Tag (TMT) 10-plex isobaric tags to label tryptic peptides [31], 2) to achieve higher coverage in labeled peptides, we reduced sample complexity by fractionating peptides prior to loading onto the LC-MS/MS, and 3) to further improve spatial specificity, we added anti-SMI312 targeted axon proximity labeling to the reference samples (in addition to NeuN and MAP2) (Fig. 2a). Confocal fluorescence imaging analysis confirmed axonal localization of anti-SMI312 targeted protein biotinylation (Supplementary Fig. 2).

Streptavidin-HRP blot analysis confirmed successful enrichment of biotinylated proteins across antibody targeted proximity labeling samples, whereas negative control samples yielded negligible signal (Supplementary Fig. 3). A total of 2,755 proteins with at least 2 unique peptides were detected in the 10-plex TMT MS experiment (Fig. 2c). The MS intensity was highly reproducible between replicates (Fig. 2d). We then used the following data analysis pipeline to refine our AIS proteome (Fig. 2c). We first identified biotinylated proteins by comparing the MS intensities of anti-NFASC samples against negative controls (-BP and -1Ab). By applying a cutoff ratio of 2, we obtained a list of 1403 biotinylated proteins. For each protein in this raw list, we calculated the ratios of its MS intensities between anti-NFASC samples versus those in the reference samples (+NeuN, +MAP2, and +SMI312). We then ranked proteins according to their averaged MS intensity ratios (+NF/+NeuN, +NF/+MAP2, and +NF/+SMI312) (Fig. 2e) and calculated their averaged rank scores (Fig. 2f). Notably, our results included many known AIS proteins (Figs

168 2e, f and 4a), including extracellular proteins (e.g. Brevican and Versican), CAMs (e.g.
169 NFASC and NRCAM), cytoplasmic proteins (e.g. NDEL1 and LIS1), and cytoskeletal or
170 cytoskeleton-associated proteins (e.g. βIV-spectrin, αII-spectrin and TRIM46). This broad
171 coverage of both cytoplasmic and cell surface proteins reflects the large labeling radius of
172 optimized IPL-AIS. Importantly, our dataset included many voltage-gated ion channels,
173 such as sodium channels (e.g. Nav1.2 and Navβ2), potassium channels (e.g. Kv7.2, Kv1.2,
174 Kv2.1 and Kvβ2), and calcium channels (e.g. Cav2.1 and Cav2.2), consistent with their roles
175 in regulating action potential initiation and shape [14].

176 AIS candidates (1403) were compared against each reference control and showed
177 their relative amounts in the AIS versus soma, somatodendritic, or axonal domains (Fig.
178 2e and Supplementary Table 2). AIS highly expressed proteins (NFASC, Nav1.2, AnkG,
179 TRIM46 and βIV-spectrin) were always ranked at the top, while more widely expressed AIS
180 proteins differentiated according to their relative expression level in subcellular domains,
181 such as the microtubule protein TUBA4A or microtubule related protein MAP6 (Fig. 2e) [17].
182 To better define AIS enriched proteins, we applied averaged rank scores to re-list the
183 known and putative AIS proteins (Fig. 2f and Supplementary Table 2). Consistently, highly
184 expressed, known AIS proteins were found among the top 5. More widely expressed
185 proteins, such as F-actin monooxygenase MICAL3 (ranked 371) and Rho GTPase activating
186 protein ARHGAP21 (ranked 455), were not as highly ranked [17].

187 To obtain a high-confidence AIS proteome list, we took the overlap of the top 200
188 proteins in each list of MS intensity ratios (+NF/+NeuN, +NF/+MAP2, and +NF/+SMI312).
189 The resulting high-confidence list contained 71 proteins (Fig. 2c, g and Supplementary
190 Table 2). Gene Ontology cellular compartment analysis revealed an over-representation
191 of AIS and node of Ranvier terms due to the similar compositions of these two
192 compartments (Fig. 2h). The remaining top 10 GOCC terms were consistent with AIS
193 characteristics and its endocytosis functions [16, 32].

194

195 **Mapping the AIS proteome across neuronal maturation**

196 The AIS is developmentally and physiologically dynamic [25, 33]. To determine dynamic
197 developmental changes in the AIS proteome, we performed IPL-AIS at DIV7, DIV14, and
198 DIV21. Two parallel 10-plex TMT experiments were performed and DIV14 samples were
199 used as a reference to bridge DIV7 and DIV21 samples (Fig. 3a).

200 We first analyzed the DIV7 AIS proteome. Parallel analysis of 1532 common proteins
201 revealed highly reproducible protein quantifications (R^2= 0.94) (Fig. 3b). After stringent
202 filtering (Supplementary Fig. 4a), we obtained 1407 biotinylated proteins. Rank analysis
203 revealed the specificity of our DIV7 AIS dataset with top ranked AIS proteins including
204 AnkG, TRIM46, βIV-spectrin, NFASC and Nav1.2 (Fig. 3c). Other AIS proteins were more
205 widely dispersed, possibly due to different expression levels and labeling efficiencies.
206 Through integrating average rank scores of AIS versus soma or somatodendrites, we
207 obtained a final ranked putative AIS proteome including AIS proteins in top positions (Fig.
208 3d and Supplementary Table 3). Using the same workflow (Supplementary Fig. 4b), we
209 identified 1738 biotinylated proteins at DIV21. Parallel analysis of anti-NFASC replicates
210 showed highly reproducible protein quantifications (R^2= 0.98) (Fig. 3e), and rank scores of
211 AIS versus soma or somatodendritic proteins (Fig. 3f) resulted in AIS proteins being
212 consistently at the top (Fig. 3g and Supplementary Table 3). Some AIS proteins, such as
213 Synaptopodin (SYNPO) and PSD-93 (PSD93) were ranked lower (Fig. 3g) [34, 35].

214 Comparing biotinylated proteins between DIV7 and DIV14 in 10-plex TMT revealed
215 173 proteins only present at DIV7 and 152 proteins only present at DIV14, among which
216 there were only two previously reported AIS proteins: Gephyrin and microtubule protein
217 TUBA4A (Supplementary Fig. 4d). DIV14 samples in the two parallel 10-plex TMT
218 experiments presented a very high reproducibility among biological replicates
219 (Supplementary Fig. 4e) and enrichment of known AIS proteins (Supplementary Fig. 4f),
220 allowing us to compare relative protein expression in three stages together. To identify the
221 core set of putative AIS proteins during development, DIV7, 14, 21 and the prior DIV14

222 datasets (Fig. 2) were combined, which generated a total of 549 common proteins (Fig.
223 3h). Among these, 534 proteins showed 20% changes in any one pair comparison of the
224 three time points and were used for heatmap clustering. Six clusters were generated with
225 distinct expression patterns (Fig. 3i and Supplementary Table 3). 51.7% of proteins were
226 gradually upregulated and 4.1% of proteins were gradually downregulated along neuronal
227 development (Fig. 3j). The cluster with the highest expression level at DIV21 included 83.5%
228 of proteins, while at DIV7 the cluster with the highest expression level included only 15.3%
229 of proteins.

230 Consistently, the previously reported AIS proteins exhibited the highest expression
231 level at DIV21, including NFASC (*Nfasc*), AnkG (*Ank3*), Nav1.2 (*Scn2a*), and βIV-spectrin
232 (*Sptbn4*), while TRIM46 (*Trim46*) decreased along neuronal development (Fig. 3k).
233 Quantitative analysis revealed the fold changes and statistical significance between stages
234 (Supplementary Table 3). For example, microtubule-associated proteins MAP1A (*Map1a*),
235 MAP6 (*Map6*), sodium/potassium-transporting ATPase subunit alpha-1 (*Atp1a1*) and
236 casein kinase II subunit alpha (*Csnk2a1*) exhibited a more than two-fold significant change
237 from DIV7 to 14 (Fig. 3l). From DIV14 to 21, more microtubule or microtubule-associated
238 proteins like TUBB5 (*Tubb5*), TUBB3 (*Tubb3*) and EB3 (*Mapre3*) significantly increased,
239 while calcium/calmodulin-dependent protein kinase KCC2D (*Camk2d*) and KCC2A
240 (*Camk2a*) also had more than two-fold changes (Fig. 3m). Comparison between DIV7 and
241 21 revealed more components with a two-fold significant increase, including the AIS
242 proteins NFASC (*Nfasc*), Nav1.2 (*Scn2a*) and GABA(A) receptor subunit gamma-2 (*Gabrg2*),
243 while TRIM46 (*Trim46*) showed a two-fold significant decrease (Fig. 3n), further
244 demonstrating the dynamic nature of AIS composition along neuronal development.
245

246 **SCRIB is a bona fide AIS enriched protein**

247 To identify novel AIS proteins, we focused on genes highly ranked in our DIV14
248 dataset but not previously reported at the AIS (Fig. 4a). Three of the top ranked hits *Wdr7*,

249 *Scrib* and *Wdr47* were selected for further analysis and to assess their subcellular
250 localization in neurons. WD repeat-containing protein 7 (WDR7) mediates V-ATPase
251 dependent vesicle acidification in kidney cell lines and neuroendocrine cells [36, 37]. In
252 neurons WDR7 may regulate synaptic vesicle acidification [38]. WDR47 is required for
253 neuronal polarization and axonal and dendritic development [39, 40]. The scaffold protein
254 SCRIB has been reported as an important regulator for apical dendrite development,
255 spine morphology, and synapse plasticity [41, 42, 43].

256 We first leveraged CRISPR/Cas9-based homology independent genome editing to
257 integrate spaghetti monster fluorescent protein with V5 tags (smFP-V5) into *Wdr7*, *Scrib*,
258 and *Wdr47* to create C-terminal fusion protein [44]. Cultured neurons were infected at DIV0
259 by AAV delivery and observed at DIV14. We found SCRIB was highly and specifically
260 enriched at the AIS, while WDR47 and WDR7 were present at the AIS, but not specifically
261 enriched there (Fig. 4b). Quantification of the smFP-V5 signal in the AIS reveals SCRIB is
262 17 ± 2.55 times higher in the AIS than in proximal dendrites, while WDR47 and WDR7 are
263 2.21 ± 0.42 and 1.12 ± 0.12 fold higher in the AIS than proximal dendrites, respectively
264 (Fig. 4c).

265 To further investigate AIS SCRIB, we treated neurons after endogenous tagging
266 (smFP-V5) of SCRIB using 0.5% TritonX-100 to reveal the detergent-resistant pool of SCRIB
267 (Fig. 5a). The detergent insoluble SCRIB was retained and highly enriched at the AIS where
268 it colocalized with the AIS cytoskeletal protein βIV-spectrin; these observations are
269 consistent with previous studies showing that AIS proteins are resistant to detergent
270 extraction [45, 46]. Some AIS proteins, including voltage gated sodium channels, βIV-spectrin,
271 NFASC and AnkG have a periodic spacing in the AIS with of approximately 180~190 nm [47,
272 48]. To test whether SCRIB also exhibits this pattern, we used stimulated emission
273 depletion (STED) nanoscopy to image smFP-V5-tagged SCRIB. We found that AIS SCRIB
274 has a periodicity of 189.4 ± 6.6 nm in DIV16 neurons (Fig. 5b). Together, these results

275 suggest a strong association of SCRIB with previously described components of the AIS
276 periodic cytoskeleton [47].

277 To determine whether SCRIB localizes to the AIS *in vivo*, we performed
278 intraventricular injection in Cas9 transgenic mice using AAV to express gRNA to target
279 endogenous mouse *Scrib* and introduce smFP-V5 into the c-terminus of SCRIB. We
280 confirmed the gRNA targeting mouse *Scrib* efficiently resulted in detection of AIS SCRIB in
281 cultured mouse hippocampal neurons (Supplementary Fig. 5a). Three weeks after
282 injection of AAV into P0 Cas9 mouse pups, we found strong V5 immunolabeling of AIS
283 that colocalized with βIV-spectrin (Fig. 5c). Thus, SCRIB is present at the AIS both *in vitro*
284 and *in vivo*.

285 To further confirm SCRIB localization at the AIS, we used commercial antibodies for
286 SCRIB labeling. We used 2 different antibodies targeting different antigens of human
287 SCRIB (amino acids 1100-1400 and 1568-1630; see methods). Consistent with our *Scrib*
288 knock-in results, antibody labeling also showed strong and specific SCRIB enrichment at
289 the AIS with and without detergent extraction (Fig. 6a and Supplementary Fig. 5b). We
290 validated the specificity of the immunostaining using CRISPR/Cas9 mediated *Scrib* knock-
291 out. We infected cultured neurons using AAV to express an HA-tag and three gRNA
292 targeting *Scrib,* or AAV expressing HA and template; transduction was performed at DIV0
293 and neurons were fixed 14 days later. SCRIB was still enriched in the AIS after transduction
294 with AAV expressing the template, but AIS labeling was lost in neurons transduced with
295 the *Scrib* gRNAs (Fig. 6b). We generated two different AAVs with 3 gRNA each targeting
296 *Scrib.* Quantification showed a ~75% and 82% reduction in AIS SCRIB positive neurons
297 after transduction with these AAVs (SCRIB positive AIS: 88.9% ± 1.5% for control, 13.7% ±
298 6.8% for *Scrib* gRNA1, and 6.7% ± 2.7% for *Scrib* gRNA2; Mean ± SEM, one-way ANOVA)
299 (Fig. 6c). In addition, loss of SCRIB did not affect AnkG clustering. We found AIS AnkG was
300 comparable in the presence or absence of SCRIB (Figs 6b, d). Finally, using the validated

301 antibodies, we found SCRIB is enriched in the AIS of neurons in cerebral cortex (Fig. 6e).
302 These results show that SCRIB is an AIS protein.
303
304 **AnkG recruits SCRIB to the AIS**
305 To determine when SCRIB becomes clustered at the AIS, we analyzed its expression
306 and distribution along neuronal development. At DIV3 we found AnkG was highly
307 enriched in the proximal axon, while SCRIB was not (Fig. 7a). By DIV7 we found clustered
308 and enriched SCRIB that colocalized with AnkG at the AIS (Fig. 7b). Quantification of SCRIB
309 and AnkG enrichment throughout development showed that AnkG was enriched in the
310 proximal axon in 52.8% ± 10.3% neurons at DIV3 and in more than 90% neurons after
311 DIV7 (Fig. 7c). In contrast, AIS SCRIB was present in only 15.1% ± 5.8% of neurons at DIV3
312 and increased to 67.8% ± 7.4%, 75.8% ± 4.4%, and 93.5% ± 2.0% at DIV7, 14, and 21,
313 respectively (Fig. 7c). These results suggest that SCRIB clustering at the AIS follows AnkG
314 clustering.
315 Previous studies show that AnkG is the earliest AIS protein and is required for AIS
316 formation and maintenance [8, 16]. To determine if AnkG also contributes to AIS clustering
317 of SCRIB, we used CRISPR/Cas9 mediated knockout of AnkG. Neurons were infected with
318 AAV expressing template or *Ank3* triple gRNA at DIV0 and then fixed at DIV14. In control
319 conditions SCRIB colocalized with AnkG. However, AIS SCRIB was not detected in AnkG
320 deficient neurons (Fig. 7d). We found a ~68% decrease of AIS AnkG positive neurons in
321 *Ank3* gRNA conditions (97.5% ± 1.4% for control; 29.4% ± 5.0% for *Ank3* gRNA conditions;
322 Mean ± SEM, p= 0.0002, unpaired t test) (Fig. 7e). Similarly, neurons with AIS SCRIB also
323 showed a ~63% decrease after loss of AnkG (94.5% ± 1.7% for control; 31.7% ± 5.8% for
324 *Ank3* gRNA conditions; Mean ± SEM, p= 0.0005, unpaired t test) (Fig. 7f). These
325 observations suggest that AnkG is necessary for SCRIB clustering at the AIS.
326 To further define the relationship between AnkG and SCRIB, we performed co-
327 immunoprecipitation (IP) experiments using HEK293T cells transfected with flag-tagged

328 SCRIB (Scrib-Flag) and GFP-tagged AnkG (AnkG270-EGFP) or pEGFP-N1. Using anti-Flag
329 antibodies, we successfully co-immunoprecipitated AnkG270-EGFP (Fig. 7g). Similarly,
330 Scrib-Flag co-immunoprecipitated with AnkG-EGFP when the latter was
331 immunoprecipitated using anti-GFP antibodies (Fig. 7h). Together, these results suggest
332 that SCRIB interacts directly with AnkG.

333 To further define how SCRIB interacts with AnkG, we used various *Scrib* truncated
334 constructs omitting N-terminal 16 leucine-rich repeats (ΔLRR), 4 PDZ domains (ΔPDZ), or
335 spacer regions between the last LRR and the first PDZ (ΔIMR) (Fig. 7i); the SCRIB was also
336 fused to dTomato. AnkG270-EGFP and truncated *Scrib* were co-transfected in HEK293T
337 cells and AnkG270-EGFP was immunoprecipitated. We found that SCRIB lacking its IMR
338 amino acids failed to interact with AnkG (Fig. 7j). In addition, compared with dTomato-
339 Scrib-ΔPDZ, dTomato-Scrib-ΔLRR had lower binding to AnkG (Fig. 7j), suggesting that the
340 N-terminus of SCRIB is critical for AnkG binding.

341

342 **DISCUSSION**

343 The AIS plays key roles in regulating action potential initiation and maintenance of
344 neuronal polarity. Functional and structural changes to the AIS in normal and pathological
345 conditions are often associated with changes in its molecular composition. Here, we used
346 IPL-AIS to identify the AIS proteome. Our experiments identified nearly all previously
347 reported AIS components including extracellular matrix proteins, membrane proteins, and
348 cytoskeleton-associated proteins. Notably, most voltage-gated ion channels and their
349 accessory subunits were also identified, including Nav1.2, Navβ2, Kv2.1, Kv7.2, Kv1.2, Kvβ2,
350 and Cav2.1 and Cav2.2 (Fig. 2f). The results reported here complement and extend a
351 previous proximity labeling study using BioID [17] especially as it relates to cell surface
352 proteins, since the prior study was biased towards cytoplasmic proteins.

353 Although we used stringent thresholding, there are likely non-AIS proteins in our
354 dataset owing to non-specific absorption of antibodies, signal amplification after

355 biotinylation, and the large labeling radius of the horse-radish peroxidase. Nevertheless,
356 our ratiometric analysis against multiple controls allowed for the strong enrichment of AIS
357 proteins including AnkG, βIV-spectrin, NFASC, Nav1.2 and TRIM46 among others (Figs 2
358 and 3). The dispersed distribution of some other known AIS proteins might be attributed
359 to their wide distribution in neurons, varied protein abundance at the AIS, or differences
360 in labeling efficiency. In addition, our control experiments may also be useful in future
361 studies to examine the relative expression of proteins in different neuronal compartments
362 (AIS, axon, dendrites and soma).

363 The AIS composition may change during neuronal development and AIS maturation.
364 For example, recent studies revealed that NuMA1 and the P2Y1 purinergic receptor
365 participate only in AIS assembly [25, 49]. We applied TMT-based quantitative mass
366 spectrometry to identify developmental changes in the AIS proteome, revealing a gradual
367 increase of most AIS proteins, including the known AIS proteins βIV-spectrin, AnkG, NFASC
368 and voltage-gated ion channels; these observations are consistent with previous analyses
369 of AIS development using immunostaining methods [33]. While as many as 83.5% of proteins
370 identified exhibited the highest level of enrichment at DIV21, we observed some proteins
371 that deviated from this general trend. For example, enrichment of the AIS protein TRIM46
372 reached its maximum at DIV7. This observation is in accordance with the proposed role of
373 TRIM46 on establishing early neuronal polarity and axon specification [13].

374 As an example of the utility of our approach to identify new AIS proteins, we
375 examined more closely the top three candidates that were not previously reported on the
376 AIS. Among them, we found SCRIB (ranked 8) is highly and specifically enriched at the AIS,
377 although all three showed some degree of enrichment. We further confirmed SCRIB's AIS
378 localization by 1) smFP-V5 tagging of endogenous SCRIB using CRISPR, 2) immunostaining,
379 3) knock-out, 4) detergent resistance, 5) periodicity like that of other AIS proteins, and 6)
380 binding to and dependence on AnkG. In the future we will perform similar analyses on
381 other candidates that are highly enriched in the AIS proteome reported here.

382 SCRIB was previously reported to regulate neuronal migration, apical dendrite
383 development, axonal connectivity and synaptic plasticity[41, 43, 50]. *SCRIB* deletion in humans
384 causes severe dysmorphic features [51], and other pathogenic variants cause neural tube
385 defects and craniorachischisis [52, 53]. Similarly, SCRIB mutants lacking the last two PDZ and
386 the C-terminal domains die before or at birth with severe brain malformation[41].
387 Heterozygous or conditional knock-out mice also show psychomotor deficits and autism-
388 like behaviors [41, 50]. However, no report has described SCRIB at the AIS. We found that
389 SCRIB's AIS localization is AnkG-dependent. Although loss of SCRIB did not affect AnkG,
390 altered AnkG expression is associated with epilepsy, and psychiatric disorders, including
391 bipolar spectrum disorder and schizophrenia [8]. Since AnkG maintains SCRIB at the AIS, we
392 speculate that loss of SCRIB function might be a core molecular pathology of AnkG-related
393 neurodevelopmental disorders. Exploring SCRIB's function at the AIS both physiologically
394 and pathologically will be of considerable interest in future studies.

395 In conclusion, the results reported here illustrate the power of IPL-AIS to define
396 molecular complexes in distinct subcellular domains. Furthermore, the results reported
397 here are a rich resource to identify other AIS-enriched proteins that may contribute to AIS
398 structure and function.

399

400 **METHODS**

401 **Animals**

402 P0 Sprague-Dawley rat pups were purchased from Peking University Health Science
403 Center. E18 pregnant Sprague-Dawley rats were purchased from Charles River
404 Laboratories. Rat pups and embryos were used for the neuron culture. P7 wild-type
405 C57BL/6 mice were purchased from Beijing Vital River Laboratory Animal Technology Co.,
406 Ltd. Transgenic Cas9 mice (JAX stock #027650) were obtained from The Jackson
407 Laboratory. P0 Cas9 pups were used for neuron culture and intraventricular injection to
408 tag endogenous *Scrib in vitro* and *in vivo*. All experimental procedures were performed in
409 accordance with the guidelines of the Institutional Animal Care and Use Committees of
410 Peking University and Baylor College of Medicine (IACUC #AN-4634).

411

412 **Probe synthesis**

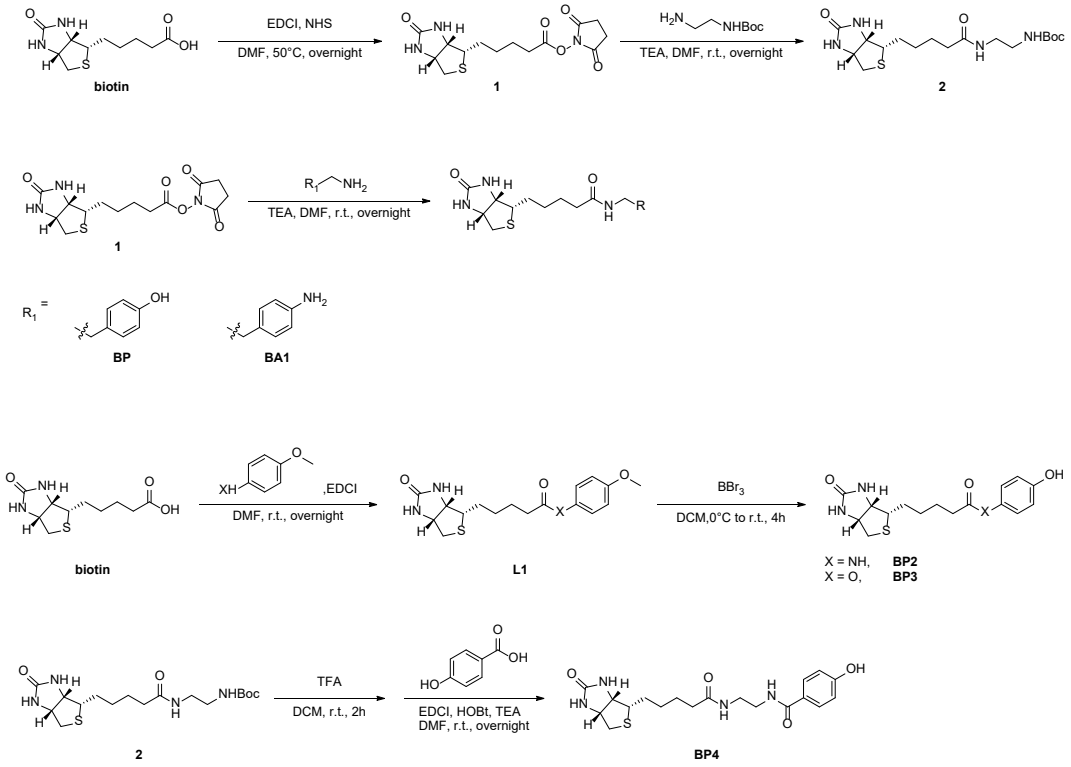

413

414

415 Synthesis of compound **1**

416 To a solution of D-biotin (1.76 g, 7.2 mmol) and EDCI (1.54 g, 8.0 mmol) in 50 ml DMF,
417 N-hydroxysuccinimide (0.92 g, 8.0 mmol) was added at room temperature (RT). The
418 reaction mixture was stirred at 50°C overnight. DMF was removed under vacuum to a
419 residue of 5 ml. Add 100 ml cold ethanol into the residue during which time a white
420 precipitate formed. Precipitate was filtered and washed with 15 ml ethanol twice, then
421 dried in vacuum to afford compound **1**. The yield was 73%.

422 ^{1}H-NMR (400 MHz, d_6-DMSO): 6.43 (1H, s), 6.37 (1H, s), 4.30 (1H, m), 4.15 (1H, m),
423 3.11 (2H, m), 2.84 (1H, dd), 2.81 (4H, s), 2.67 (2H, t), 2.60 (1H, d), 1.75-1.30 (6H, m).

424

425 Synthesis of compound **2**

426 Trimethylamine (1.60 g, 16 mmol) was added to a solution of mono-Boc protected
427 ethylene diamine (1.66 g, 10 mmol) and compound **1** (1.76 g, 5.2 mmol) in 50 ml DMF.
428 The reaction mixture was stirred at RT overnight and concentrated by rotary evaporation.
429 The residue was dissolved in a solution of DCM and ^{i}PrOH (v/v = 4:1) and washed with 20
430 ml 1 M HCl followed by 20 ml water three times. The organic layers were combined and
431 evaporated, and the residue was purified by column chromatography, affording
432 compound **2**. The yield was 72%.

433 ^{1}H-NMR (400 MHz, d_6-DMSO): 7.79 (1H, t), 6.79 (1H, t), 6.43 (1H, s), 6.36 (1H, s), 4.30
434 (1H, m), 4.13 (1H, m), 3.05 (3H, m), 2.96 (2H, m), 2.81 (1H, dd), 2.59 (1H, d), 2.04 (2H, t),
435 1.68-1.41 (4H, m), 1.37 (9H, s), 1.34- 1.19 (2H, m).

436

437 Synthesis of **BP** and **BA1**

438 To a solution of compound **1** (0.50 g, 1 e.q.) and corresponding primary amine (1.1
439 e.q.) in 50 ml DMF, trimethylamine (3 e.q.) was added to the mixture and stirred overnight
440 at RT. The reaction solvent was evaporated and the residue was purified by C18 reverse
441 phase column (Waters XBridge Prep C18 5 µm OBD 19x150 mm) on semi-preparative

UPLC (Waters 2998 Photodiode Array Detector and 2545 Binary Gradient Module) with a gradient of 3% to 60% methanol in water over 25 min. The overall yields were 60-70%.

^{1}H-NMR for **BP** (400 MHz, d_6-DMSO): 9.13 (1H, s), 7.79 (1H, t), 6.97 (2H, d), 6.66 (2H, d), 6.42 (1H, s), 6.35 (1H, s), 4.31 (1H, m), 4.12 (1H, m), 3.18 (2H, dd), 3.08 (1H, m), 2.83 (1H, dd), 2.57 (3H, m), 2.03 (2H, t), 1.65-1.39 (4H, m), 1.35-1.19 (2H, m).

^{1}H-NMR for **BA1** (400 MHz, d_6-DMSO):7.78 (1H, t), 6.84 (2H, d), 6.49 (2H, d),6.43 (1H, s), 6.36 (1H, s), 4.85 (2H, s), 4.31 (1H, m), 4.12 (1H, m), 3.16 (2H, dd), 3.09 (2H, dd),2.84 (1H, dd), 2.56 (3H, m), 2.03 (2H, t), 1.38-1.66 (4H, m), 1.28 (2H, m).

Synthesis of **BP2** and **BP3**

To a solution of D-biotin (1.00 g, 4.0 mmol), EDCI (0.85 g, 4.5 mmol) in 30 ml DMF, corresponding phenol or aniline (0.56 g, 4.5 mmol) was added and the reaction mixture was stirred at RT overnight. The reaction mixture was evaporated, and the residue was purified by column chromatography, affording compound **L1**.

To the solution of **L1** in 20 ml DCM, BBr_3 (1.0 ml, 10 mmol) was added to the mixture dropwise at 0°C. After being stirred at 0°C for 4 h, the mixture was heated to RT and continued to react for 12 h. Then, 50 ml water was added to the mixture, and the residue was washed by 10 ml cold water for three times, and purified by semi-preparative column to get the purified product **BP2** or **BP3**. The whole yield was 25%.

^{1}H-NMR for **BP2** (400 MHz, d_6-DMSO): 9.60 (s, 1H), 9.13 (s, 1H), 7.35 (d, 2H), 6.67 (d, 2H), 6.45 (s, 1H), 6.37 (s, 1H), 4.31 (m, 1H), 4.14 (m, 1H), 3.14 (m, 1H), 2.84 (dd, 1H), 2.59 (d, 1H), 2.25 (t, 2H), 1.69-1.46 (m, 4H), 1.42-1.27 (m, 2H).

^{1}H-NMR for **BP3** (400 MHz, d_6-DMSO): 9.44 (s, 1H), 6.90 (m, 2H), 6.76-6.74 (m, 2H), 6.47 (s, 1H), 6.38 (s, 1H), 4.31 (m, 1H), 4.15 (m, 1H), 3.13 (m, 1H), 2.83 (dd, 1H), 2.58 (d, 1H), 2.53 (m, 2H), 1.71-1.47 (m, 4H), 1.45-1.34 (m, 2H).

Synthesis of **BP4**

469 Compound **2** (0.45 g, 1.2 mmol) was dissolved in 15 ml TFA/DCM (v/v= 1:1) and
470 stirred at RT for 2 h. The solvent was removed under vacuum and the residue was
471 dissolved in 20 ml DMF. To this solution was added 4-Hydroxybenzoic acid (0.15 g, 1.2
472 mmol), EDCI (0.45 g, 2.4 mmol), HOBt (0.35 g, 2.4 mmol), and TEA (0.36 g, 3.5 mmol). The
473 reaction mixture was stirred at RT overnight. Then, the reaction mixture was evaporated,
474 and the residue was purified by C18 reverse phase column (Waters XBridge Prep C18 5
475 µm OBD 19x150 mm) on semi-preparative UPLC (Waters 2998 Photodiode Array Detector
476 and 2545 Binary Gradient Module) with a gradient of 3% to 80% methanol in water over
477 30 min. The overall yields were 50%.
478 ^{1}H-NMR (400 MHz, d_6-DMSO): 8.21 (t, 1H), 7.90 (t, 1H), 7.69 (d, 2H), 6.85 (d, 2H),
479 6.39 (d, 2H), 4.29 (dd, 1H), 4.14 (m, 1H), 3.03 (ddd, 1H), 2.80 (dd, 1H), 2.57 (d, 1H), 2.06
480 (t, 2H), 1.67-1.19 (m, 6H).
481
482 **Primary neuron culture**
483 Neurons were prepared from cortices or hippocampi of embryos and P0 pups.
484 Tissues were dissected and incubated in a digestion solution (0.25% trypsin and 0.4 mg/ml
485 DNase in Ca^{2+}/Mg^{2+} free HBSS) at 37°C for 15 min. Followed by the dissociation, neurons
486 were plated onto 100 µg/ml poly-D-lysine (Sigma) coated 10-cm dishes at a density of
487 100,000 cells/cm^2 or on coverslips coated by 20 µg/ml poly-D-lysine and 10 µg/ml laminin
488 mouse protein (Gibco) at a density of 40,000 cells/cm^2 in plating medium (high glucose
489 DMEM medium containing L-glutamine and 10% fetal bovine serum). After 3 h, the
490 medium was changed into neuronal culture medium (Neurobasal, B27 supplement,
491 Glutamax-I and penicillin-streptomycin) to maintain neuronal long-term growth. 2 µM
492 cytosine β-D-arabinofuranoside hydrochloride (AraC) was added after 6 days to slow
493 down glia cells proliferation. One third of culture medium was replaced with fresh
494 neuronal culture medium every seven days.
495

496 **Optimization of anti-NFASC antibody directed AIS proximity labeling**

497 Neurons were fixed with 4% formaldehyde for 15 min at RT. The free aldehyde group
498 was quenched by 0.25 M Glycine for 10 min. After washing four times with PBS,
499 endogenous peroxidase of cells was deactivated in 1.5% H_2O_2 as long as 1.5 h. Washed
500 samples were blocked by 5% fetal bovine serum dissolved in PBS containing 0.1% Tween-
501 20 for 1 h at RT. Then neurons were stained with 1, 2 or 5 μg/ml mouse anti-Pan-
502 Neurofascin (anti-NFASC, NeuroMab, Cat# 75-172, stock 1 mg/ml) dissolved in antibody
503 dilution solution (1% FBS with 0.1% Tween-20 in PBS) for 1 h at RT. Followed by washes
504 in washing solutions (0.1% Tween-20 in PBS), samples were labelled with 0.1, 0.2, 0.5 or
505 1 μg/ml HRP conjugated anti-mouse IgG (Cell signaling technology, Cat# 7076S, stock 1
506 mg/ml) for 1 h. Samples were washed for another four times with washing solution and
507 incubated with 6 different probes (see Supplementary Fig. 1e) individually at a
508 concentration of 500 μM for 10 min. The proximity labeling was triggered with the
509 addition of H_2O_2 (1, 100, 500 or 1000 μM). After 1, 5 or 10-min reaction, the proximity
510 labeling was stopped by adding quenching solutions (50 mM sodium ascorbate and 5 mM
511 Trolox dissolved in PBS). Endogenous bait protein NFASC and biotinylated proteins were
512 detected by immunocytochemistry to compare proximity labeling specificity and
513 efficiency through microscopy.

514

515 **Immunoproximity labeling**

516 The above optimized parameters were applied to anti-NFASC, anti-NeuN, anti-MAP2
517 and anti-SMI312 directed proximity labeling to capture AIS, soma, somatodendrites and
518 axon components. The blocked samples were stained with primary antibodies dissolved
519 in antibody dilution solution (1% FBS with 0.1%Tween-20 in PBS) for 1 h at RT. After
520 washing, samples were labelled with HRP conjugated second antibodies for 1 h and then
521 incubated with 500 μM biotin-phenol (BP) for 10 min. The proximity labeling was
522 triggered with the addition of 100 μM H_2O_2. After 1 min reaction, free radicals were

523 quickly quenched twice by quenching solutions (50 mM sodium ascorbate and 5 mM
524 Trolox dissolved in PBS). Samples were finally washed with PBS.
525 In the case of anti-AnkG and anti-TRIM46 targeted proximity labeling, parameters
526 including antibody dilutions and H_2O_2 concentration were also individually tested.
527 Antibodies used for proximity labeling were listed as follows. Primary antibodies: mouse
528 anti-Pan-Neurofascin (anti-NFASC, NeuroMab, Cat# 75-172), mouse anti-AnkG
529 (NeuroMab, Cat# 75-146), mouse anti-NeuN (Abcam, Cat# ab104224), mouse anti-MAP2
530 (Sigma-Aldrich, Cat# M1406), mouse anti-Neurofilament (anti-SMI312, Biolegend, Cat#
531 837904), chicken anti-AnkG (Synaptic Systems, Cat# 386006) and chicken anti-TRIM46
532 (Synaptic Systems, Cat# 377006). HRP conjugated second antibodies: anti-mouse IgG (Cell
533 signaling technology, Cat# 7076S) or anti-chicken IgY (Invitrogen, Cat# A16054; Abcam,
534 Cat# ab6877).
535
536 **Protein lysis of cortical neurons after proximity labeling**
537 Dimethyl experiments include three pairs: anti-NFASC vs. no primary antibody; anti-
538 NFASC vs. anti-NeuN; and anti-NFASC vs. anti-MAP2. Three times independent replicates
539 were performed in each pair. The 10-plex TMT DIV14 MS experiment include: three
540 biological replicates for anti-NFASC targeted proximity labeling; no primary antibody or
541 BP probe negative controls; reference samples of anti-NeuN, anti-MAP2 (duplicates), and
542 anti-SMI312 (duplicates). Due to differences in the bait abundance, references samples
543 of anti-NeuN, anti-MAP2 and anti-SMI312 yielded higher amounts of labeled proteins
544 than the anti-NFASC sample. To balance peptide loading to LC-MS/MS analysis, we used
545 only a fraction of the reference samples for biotinylated proteins enrichment. Anti-NF186,
546 no primary antibody and no substrate BP shared the same protein quantity for
547 enrichment. 1/2 protein quantity was used for anti-NeuN enrichment and 1/4 amount
548 was used for anti-MAP2 and anti-SMI312 enrichment respectively.

549 In AIS developmental TMT experiments, two parallel 10-plex TMT experiments were
550 performed and DIV14 samples were used as a reference for DIV7 and DIV21 samples.
551 Proximity labelled samples at DIV14 were equally divided and used for TMT1 and TMT2
552 pipeline. Five conditions were designed for each stage: anti-NFASC targeted AIS proximity
553 labeling (duplicates); no primary antibody (-1Ab); anti-NeuN targeted soma proximity
554 labeling and anti-MAP2 targeted somatodendrites proximity labeling. An amount of 1.5
555 mg proteins in samples of anti-NFASC and no primary antibody (DIV7, 14 and 21) were
556 used for enrichment, while 1/2 and 1/4 protein quantity were used for anti-NeuN and
557 anti-MAP2 enrichment individually.

558 Proximity labeling samples were lysed with lysis solution (50 mM Tris-HCl pH 7.6, 150
559 mM NaCl, 1% SDS, 0.5% sodium deoxycholate, 1% Triton X-100 and protease inhibitors
560 cocktail) on ice for 10 min. 500 µl lysis solution was added for each 10-cm dish. In the
561 condition of anti-NFASC, no primary antibody and no substrate BP, three 10-cm dishes in
562 one replicate were needed for protein lysis. While for anti-NeuN, anti-MAP2 and anti-
563 SMI312 conditions, one or two 10-cm dishes were needed. Protein lysis were de-
564 crosslinked at 99ºC for 1 h. The lysed solution was sonicated on ice and then centrifuged
565 at 12,000 rpm for 10 min at 4ºC to collect supernatant. Proteins were precipitated in cold
566 methanol at -80ºC.

567

568 **Enrichment of biotinylated proteins and on-bead digestion**

569 Precipitated proteins were washed twice using cold methanol. Purified proteins
570 were dissolved completely in 0.5% SDS (w/v). Protein concentrations were measured
571 using a BCA Protein Assay Kit to adjust protein quantity for enrichment. 1% of pre-
572 enrichment proteins were kept to test biotinylated signal via Western blotting or silver
573 staining to assess proximity labeling efficiency. The remaining proteins were incubated
574 with 200 µl streptavidin beads for 3 h with gentle rotation at RT. 5% of post-enrichment
575 proteins were kept to test the enrichment efficiency via Western blotting or silver staining.

576 Then the protein-beads mixture was sequentially washed twice by 2% SDS (w/v), 8 M urea
577 and 2 M sodium chloride. The mixture was reduced by 10 mM dithiothreitol and then with
578 20 mM iodoacetamide for alkylation. After washing four times with 100 mM TEAB,
579 proteins on beads were digested with the addition of 2 μg trypsin (Promega, Cat# V511A)
580 for 18 h at 37°C.
581
582 **Immunoblotting and silver staining**
583 Protein samples were heated at 99°C for 10 min with the addition of reducing
584 Laemmli SDS loading buffer. In the case of post-enrichment biotinylated protein samples,
585 2 mM biotin was added to elute biotinylated proteins. In the case of co-
586 immunoprecipitation (IP) experiments, AnkG270-EGFP or pEGFPN1 were co-transfected
587 with Scrib-Flag or its truncation variants in HEK293T cells and lysed after 48 h. The Scrib-
588 Flag plasmid was generated by amplifying human *Scrib* coding sequence from MSCV Puro
589 SCRIB WT (Addgene, Cat# 88886) and fused with 3xFlag tag at the C-terminal in pcDNA3
590 backbone. AnkG270-GFP was a kind gift from Dr. Vann Bennett (Duke University). The *Scrib*
591 truncation mutants dTomato-Scrib-ΔLRR, dTomato-Scrib-ΔIMR, and dTomato-Scrib-ΔPDZ
592 were kind gifts from Maya Shelly (Stony Brook University).

593 Input and immunoprecipitated samples were dissolved in Laemmli buffer (62.5 mM
594 Tris-HCl (pH 6.8), 2% SDS, 10% Glycerol, 2% 2-Mercaptoethanol, and 0.005% Bromophenol
595 blue) for immunoblotting. Proteins were loaded for electrophoresis in 5% SDS-PAGE
596 stacking gel. 10% or 6% SDS-PAGE separating gels were used for biotinylated samples and
597 co-IP samples respectively. The blots were blocked with 5% BSA at RT for 1 h and then
598 sequentially labeled using primary antibodies and HRP conjugated secondary antibodies.
599 Antibodies used were: rabbit anti-GFP (Invitrogen, Cat# A11122), chicken anti-GFP (Aves
600 Labs, Cat# GFP-1020), mouse anti-Flag (MBL, Cat# M185-3L), chicken anti-mCherry (Aves
601 Labs, Cat# MCHERRY-0020), rabbit anti-Flag conjugated with HRP (Cell Signaling, Cat#
602 86861), streptavidin-HRP (Invitrogen, Cat# 21124), goat anti-mouse IgG (H+L) conjugated

603 with HRP (Jackson, Cat# 115-035-146), goat anti-rabbit IgG (H+L) conjugated with HRP
604 (Jackson, Cat# 111-035-003), and goat anti-chicken IgY conjugated with HRP (Aves, Cat#
605 H-1004). The blots were developed by Clarity western ECL substrate (Bio-Rad, Cat#
606 1705060) and imaged in ChemiDoc MP Imaging System (Bio-Rad). In addition, the SDS-
607 PAGE gels could be directly used for silver staining using the Fast Silver Stain Kit (Beyotime,
608 Cat# P0017S).

609

610 **Dimethyl labeling**

611 Enriched proteins were digested with trypsin and the resulting peptides were treated
612 with isotope-encoded formaldehyde (heavy $D^{13}CDO$ for anti-NFASC samples and light
613 HCHO for negative control/reference samples) and $NaBH_3CN$ for their $–NH_2$ groups
614 methylation, resulting in a mass shift from 34.0631 Da to 28.0313 Da. For pairs of anti-
615 NFASC and no primary antibody, peptides were combined directly and desalted by C18
616 tips (ThermoFisher, Cat#87784). For pairs of anti-NFASC/ anti-NeuN or anti-NFASC/ anti-
617 MAP2, peptides were desalted first separately and then equal amounts of peptides were
618 combined. Peptides concentration was measured by Quantitative Colorimetric Peptide
619 Assay Kit (ThermoFisher, Cat# 23275). Combined peptides were dried in a vacuum
620 concentrator and ready for liquid chromatography-tandem mass spectrometry (LC-
621 MS/MS).

622

623 **10-plex TMT labeling and peptides fractionation**

624 Digested peptides were desalted by C18 tips (ThermoFisher, Cat#87784). In the case
625 of 14 DIV independent TMT experiments, desalted total peptides of anti-NF186, no
626 primary antibody and no substrate BP were directly used for TMT labeling. Taking anti-
627 NF186 peptides amount as reference, the same quantity of peptides from anti-NeuN,
628 anti-MAP2 and anti-SMI312 conditions were prepared in advance. Peptide concentration
629 was measured by Quantitative Colorimetric Peptide Assay Kit (ThermoFisher, Cat# 23275).

630 In the case of AIS developmental TMT experiments, sample amount was controlled when
631 performing enrichment. Therefore, these peptides were directly applied to TMT labeling.
632 TMT labeling was performed as instructed by TMT 10-plex Mass Tag Labeling Kits
633 and Reagents (ThermoFisher, Cat# 90110). Briefly, TMT reagents were maintained at RT
634 and reconstituted with 41 µl anhydrous acetonitrile for 0.8 mg vial of each tag. Peptides
635 were reconstituted in 10 µl 100 mM TEAB and dissolved completely. Add 12.5 µl TMT
636 solution into dissolved peptides and label for 2 h in the dark. The labeling in each
637 condition was described in Figs 2b and 3a. The reaction was quenched by adding 8 µl 5%
638 hydroxylamine and which was incubated for 15 min. Peptides from ten conditions were
639 mixed and dried in a vacuum concentrator. Mixed peptides were re-dissolved in 300 µl
640 0.1% trifluoroacetic acid and fractionated according to the instructions of Pierce High pH
641 Reversed-Phase Peptide Fractionation Kit (ThermoFisher, Cat# 84868). Samples were
642 eluted by gradient acetonitrile of 10.0%, 12.5%, 15.0%, 17.5%, 20.0%, 22.5%, 25.0%, 50.0%
643 solution in 0.1% triethylamine and defined as fraction 1-8 respectively. Fractions were
644 combined as pairs of '1+5', '2+6', '3+7' and '4+8' and dried again in vacuum concentrators.
645 Peptides were ready for LC-MS/MS.
646
647 **Liquid chromatography and mass spectrometry**
648 Peptides were reconstituted in 0.1% formic acid and separated in a loading column
649 (100 µm × 2 cm) and a C18 separating capillary column (75 µm × 15 cm) packed in-house
650 with Luna 3 µm C18(2) bulk packing material (Phenomenex, USA). A 2-h liquid
651 chromatography (LC) was applied to peptides separation. The LC gradient was held at 2%
652 for the first 8 minutes of the analysis, followed by an increase from 2% to 10% B from 8
653 to 9 minutes, an increase from 10% to 44% B from 9 to 123 minutes, and an increase from
654 44% to 99% B from 123 to 128 minutes (A: 0.1% formic acid in water and B: 80%
655 acetonitrile with 0.1% formic acid).

656 Samples were analyzed by Orbitrap Fusion LUMOS Tribrid Mass Spectrometer. The
657 precursors were ionized using an EASY-Spray ionization source (Thermo Fisher Scientific).
658 Survey scans of peptide precursors were collected in the Orbitrap from 350-1600 Th with
659 an advance gain control (AGC) target of 400,000, a maximum injection time of 50 ms, RF
660 lens at 30%, and a resolution of 60,000 at 200 m/z. In the case of HCD scans, an automated
661 scan range determination was enabled. An isolation window of 1.6 Th was used to select
662 precursor ions with the quadrupole. Product ions were collected in the Orbitrap with the
663 first mass of 110 Th, an AGC target of 50,000, a maximum injection time of 30 ms, HCD
664 collision energy at 30%, and a resolution of 15,000. Monoisotopic precursor selection was
665 enabled for peptide isotopic distributions, precursors of z = 2-7 were selected for data-
666 dependent MS/MS scans for 3 s of cycle time, and dynamic exclusion was set to 15 s with
667 a ±10 ppm window set around the precursor mono-isotope.
668

669 **Mass spectrometry data analysis**

670 Raw data files were loaded in MaxQuant software (version 1.6.10.43) and searched
671 against Rattus norvegicus proteomes from uniprot database (Taxonomy, 10116,
672 downloaded on Nov 15th, 2020). Trypsin was selected as the digestion mode. In the case
673 of searching dimethyl proteomics, the composition of Hx(6)C(2)H(-2) was replaced by
674 Hx(4)Cx(2) in heavy labels of DimethLys6 and DimethNter6. Cysteine acetylation
675 (carbamidomethyl) was a fixed modification. Methionine oxidation and protein N-
676 terminal acetylation were variable modifications. Re-quantify button in Misc. module and
677 match between runs in Identification module were activated. In the case of 10-plex TMT
678 proteomics, reporter ion MS2 was selected and 10-plex TMT was activated. Correction
679 factors were added to the tags based on the reagent instructions (ThermoFisher, Cat#
680 90110, Lot: UL291038). In both cases, the false discovery rate was set to 0.01.
681

682 **Proteome data analysis**

683 Anti-NFASC targeted AIS proximity labeling was the positive group. Samples of no
684 primary antibody or no substrate BP were negative controls for cutoff analysis, while anti-
685 NeuN, anti-MAP2 or anti-SMI312 targeted soma, somatodendrites or axon proximity
686 labeling were reference controls for ranking AIS candidates. Top ranked proteins would
687 have more possibility to be expressed or enriched in the AIS.

688 In the case of dimethyl experiments, contaminants and proteins identified as
689 reversed hits were removed. Proteins containing at least 2 unique peptides and quantified
690 in at least two out of three independent replicates were retained for further analysis (anti-
691 NFASC vs. anti-NeuN: 965; anti-NFASC vs. anti-MAP2: 802). Additionally, an H/L ratio > 1.5
692 was set as the cutoff for each replicate in the experiment of anti-NFASC versus no primary
693 antibody, which resulted in the identification of 704 proteins. Proteins in three pairs were
694 intersected and a total of 568 proteins were obtained. We normalized the H/L ratio
695 against the medium in each column using the formula of '$\log_2$(H/L)-medium $\log_2$(H/L)' in
696 +NFASC/+NeuN and +NFASC/+MAP2 replicates. Averaged normalized data was obtained
697 from three replicates and used for distribution analysis.

698 In the case of DIV14 TMT experiments, contaminants and proteins identified as
699 reversed hits were removed. Proteins with at least two unique peptides were kept. Ratios
700 were calculated by division using their MS intensity. Parallel analysis was analyzed using
701 Pearson correlation. The average ratio of replicates was used for the following analysis.
702 The cutoff ratio was set at 2 for +NFASC/-BP and +NFASC/-1Ab. A total of 1403 proteins
703 were retained for further analysis. Ratios of +NFASC/+NeuN, +NFASC/+MAP2 and
704 +NFASC/+SMI312 were normalized against the medium ratio in their corresponding
705 column. Proteins were ranked based on average normalized $\log_2$(+NFASC/+References,
706 fold change) in a descending order. The final overall rank was based on the average rank
707 scores against soma, somatodendrites and axon. Proteins in the top 200 against each
708 reference were overlapped and a total of 71 proteins were obtained. Gene Oncology
709 analysis of these 71 proteins was performed PANTHER overrepresentation test. A total of

710 2755 neuronal proteins in this TMT were used as a reference. Among them, 2744 proteins
711 were valid data in Gene Oncology database. Top 10 cellular compartment terms were
712 presented.

713 In the case of AIS developmental TMT experiments, two parallel 10-plex TMT labeling
714 were employed to analyze AIS developing (DIV7), mature (DIV14) and completely mature
715 (DIV21) proteome changes. Contaminants and proteins identified as reversed hits were
716 removed. Proteins with at least two unique peptides were kept. Ratios were calculated
717 by division using their MS intensity. Parallel analysis was analyzed using Pearson
718 correlation. The average ratio of replicates was used for further analysis. Proteins were
719 filtered with the standard of 'average $\log_2$(+NFASC)-$\log_2$(-NFASC)>3.5' for DIV7 and 21,
720 while for DIV14 the standard was set as 'average $\log_2$(+NFASC)-$\log_2$(-NFASC)>1'. This
721 setting was based on the endogenous biotinylated proteins distribution. Proteins with
722 intensity in +NFASC condition, not in -NFASC condition were also retained. Ratios of
723 +NFASC/+NeuN and +NFASC/+MAP2 were normalized against the medium ratio in their
724 corresponding column in each time point. Proteins were ranked based on average
725 normalized $\log_2$(+NFASC/+References, fold change) in a descending order. The final
726 overall rank was based on the average rank scores against soma and somatodendrites.

727 For analysis of AIS protein dynamics along neuronal development, biotinylated
728 proteins at DIV7, 14 and 21 together with prior DIV14 biotinylated proteins were
729 overlapped and revealed 549 common proteins in three stages. These proteins in the
730 condition of anti-NFASC at DIV7, 14 and 21 were normalized based on endogenous
731 biotinylated protein PCCA [54]. Among 549 proteins, 534 proteins were presented more
732 than 20% changes of average MS intensity in at least one pair of time points. Heatmap
733 was performed using cutree script in R package of pheatmap. AIS molecules identified in
734 three stages were performed Z-scored normalized abundance analysis. Significant
735 analysis and fold changes were analyzed regarding these AIS proteins according to a guide
736 of statistics for proteomics data analysis [55].

737

738 **Immunocytochemistry and immunohistochemistry**

739 For immunocytochemistry, neurons were fixed in 4% formaldehyde for 15 min at RT
740 and washed three times in PBS. Samples were blocked by 5% fetal bovine serum dissolved
741 in PBS containing 0.1% Tween-20 for 1 h at RT. Then neurons were sequentially stained
742 with primary antibodies and fluorescent second antibodies for 1 h at RT. Nuclei were
743 stained with DAPI (Invitrogen, Cat# D1306). In the case of detergent extraction
744 experiments, neurons were treated with 0.5% Triton X-100 in PBS for 5 min at RT before
745 fixation.

746 Primary antibodies used for immunocytochemistry in this study were: mouse anti-
747 Pan-Neurofascin (NeuroMab, Cat# 75-172, 1:1000), mouse anti-AnkG (NeuroMab, Cat#
748 75-146, 1:1000), chicken anti-AnkG (Synaptic Systems, Cat# 386006, 1:500), guinea pig
749 anti-AnkG (Synaptic Systems, Cat# 386004, 1:1000), mouse anti-NeuN (Abcam, Cat#
750 ab104224, 1:1000), mouse anti-Neurofilament (Biolegend, Cat# 837904, 1:1000), mouse
751 anti-MAP2 (Sigma-Aldrich, Cat# M1406, 1:1000), chicken anti-MAP2 (Abcam, Cat# ab5392,
752 1:10000), chicken anti-MAP2 (EnCor Biotechnology, Cat# CPCA-MAP2, 1: 2000), chicken
753 anti-TRIM46 (Synaptic Systems, Cat# 377006, 1:500), rabbit anti-βIV-spectrin (laboratory
754 of Dr. Matthew Rasband in BCM, 1:1000), rabbit anti-SCRIB (Abclonal, Cat# A17450, 1:50),
755 rabbit anti-SCRIB (Invitrogen, Cat# PA5-28628, 1:100), mouse anti-V5 (Invitrogen, Cat#
756 R960CUS, 1:500) and rat anti-HA (Millipore Sigma, Cat# 11867423001, 1:1000).
757 Fluorescent second antibodies were: goat anti-mouse IgG2a, Alexa Fluor 488 (Invitrogen,
758 Cat# A21131); goat anti-mouse IgG (H+L), Alexa Flour 488 (Invitrogen, Cat# A11029), 568
759 (Invitrogen, Cat# A11031), and Plus 594 (Invitrogen, Cat# A32742); goat anti-rabbit IgG
760 (H+L), Alexa Flour 488 (Invitrogen, Cat# A11034), and 568 (Invitrogen, Cat# A11036); goat
761 anti-rat IgG (H+L), Alexa Flour 594 (Invitrogen, Cat# A11007); goat anti-chicken IgY (H+L),
762 Alexa Flour 488 (Invitrogen, Cat# A11039), 647 (Invitrogen, Cat# A21449), and AMCA
763 (Jackson, Cat# 103-155-155). In the case of proximity labeling samples, biotinylated

764 protein signal was detected by incubation with streptavidin conjugated with Alexa Fluor
765 568 (Invitrogen, Cat# S11226) or 647 (Invitrogen, Cat# S21374).
766 For immunohistochemistry, brain sections of P7 C57BL/6 mice or P23 Cas9 mice
767 tagged with smFP-V5 to *Scrib* were used for the staining. Cortical sections were blocked
768 for 2 h at RT in 10% fetal bovine serum dissolved in PBS containing 0.1% TritonX-100 and
769 then incubated with first antibodies at 4°C overnight. After washing, slices were incubated
770 with second antibodies and counterstained with DAPI. First antibodies used were: mouse
771 anti-AnkG (NeuroMab, Cat# 75-146, 1:500), rabbit anti-SCRIB (Abclonal, Cat# A17450,
772 1:50), mouse anti-V5 (Invitrogen, Cat# R960CUS, 1:500), and rabbit anti-βIV-spectrin
773 (laboratory of Dr. Matthew Rasband in BCM, 1:500). Second antibodies used were: goat
774 anti-mouse IgG (H+L), Alexa Flour 568 (Invitrogen, Cat# A11031), goat anti-rabbit IgG
775 (H+L), Alexa Flour 488 (Invitrogen, Cat# A11034), and 568 (Invitrogen, Cat# A11036), and
776 goat anti-mouse IgG2a, Alexa Fluor 488 (Invitrogen, Cat# A21131). Sections were
777 mounted to glass slides with Fluoromount-G (SouthernBiotech, Cat# 0100-01).
778 Images were acquired on an inverted fluorescence microscope (Nikon-TiE, Japan)
779 equipped with a 40x1.3 NA oil immersion objective lens, confocal laser lines (OBIS 405,
780 488, 532, 561 and 637 nm, Coherent, USA), spinning disk confocal unit (Yokogawa CSU-
781 X1, Japan) and scientific CMOS cameras (Hamamatsu ORCA-Flash 4.0 v2). The microscope,
782 camera and lasers were controlled with a customer-built software written in LabVIEW
783 (National Instruments). Sections were imaged in the focal position or in z-stacks with a
784 0.5 µm step size at a resolution of 1500x1000 pixels. Z-projection was obtained in Fiji-
785 ImageJ software. Figures were adjusted and prepared in Fiji-ImageJ and Adobe Photoshop
786 CC2018.
787
788 **V5 tag knock-in and microscopy**
789 V5 tag knock-in sgRNA and donor constructs were generated following previously
790 described strategies [44, 56]. The specific target sequences of guide RNA (gRNA) were

designed for knock-in: rat *Scrib* 5'-GGGAAGCACCTGGCCCTAGG-3'; rat *Wdr47* 5'-TCTGGACTTACAGTGGCTAG-3'; rat *Wdr7* 5'-ACGGCAGTCAGACCATGAAG-3'; mouse *Scrib* 5'-GTCCCGGCCGCACAGACCGA-3'. Plasmids of gRNA or AAV-SpCas9 (Addgene# 60957, Dr. Feng Zhang) together with pUCmini-iCAP-PHP.S (Addgene# 103002, Dr. Viviana Gradinaru) and pHelper (Cat #240071, Agilent Technologies) were used for AAV production. Adeno-associated virus (AAV) cell-lysates were produced using the AAVpro Purification Kit (All Serotypes) (Takara) with slight modifications. Briefly, HEK293T cells were transfected with AAV plasmid, helper plasmid, and serotype PHP.S plasmid and collected after three days. The cells were lysed using the AAV Extraction Solution A plus and B, and this crude AAV solution was used for neuronal *in vitro* transduction. An aliquot of 20 µl AAVs (10 µl of Cas9 and 10 µl of knock-in sgRNA and donor) was added to a well of 12-well plates at DIV0. The medium was replaced after two days of infection. Neurons were fixed at the indicated time points for immunocytochemistry. Concentrated AAV solution of smFP-V5 knock-in to mouse *Scrib* was used for AAV intraventricular injection on P0 Cas9 mice pups. 50~100 µl AAV was concentrated from 2x15-cm dishes and 2 µl was used for each hemisphere.

Imaging was performed using a Zeiss AxioImager Z2 fitted with apotome for structured illumination. Images were captured using the Zeiss ZEN software. Super-resolution images were performed by Stimulated Emission Depletion (STED) microscope using a STEDyCON (Abberior) system fitted to a Nikon Eclipse Ti2 microscope. The periodicity of SCRIB was measured in Fiji-ImageJ after generating a line scan across the AIS. The distance between peak fluorescence intensities (maximum to maximum) was then measured.

Genes knock-out and imaging by microscopy

Triple gRNAs for rat *Scrib* and *Ank3* were designed: *Scrib* gRNA1 (5'-GCTATTGAACTTGCGGAAGT-3', 5'-CCAGGCATACCAGCCGCCGC-3', and 5'-CTGTGAGGATCAGTTCCGAG-3'); *Scrib* gRNA2 (5'-AGCCACAGCTCCCGTAGGTT -3', 5'-

818 GGCTAACTTCATGCAACTGG-3', and 5'-TTATGCTCTCAGGTATCTCG-3'); *Ank3* gRNA (5'-
819 CTGCTCGAGAACGACACGAA -3', 5'-CGCTCGGTTTAACAGCAACG -3', and 5'-
820 CTTCACGCCGCTGTATATGG-3'). The plasmid backbone consists of a cassette of synapsin1
821 promoted tandem HA tag as indicator for transfection. Crude AAV virus were generated
822 by co-transfection of AAV plasmid, helper plasmid, and serotype PHP.S plasmid in
823 HEK293T cells. An aliquot of 20 µl AAVs (10 µl of Cas9 and 10 µl of knock-out sgRNAs) was
824 added to a well of 12-well plates at DIV0. Neurons were fixed at DIV14 and stained for
825 imaging using a Zeiss structured illumination microscope with apotome.
826
827 **Image analysis:**
828 Cortical neurons of DIV10-14 were processed for optimizing AIS proximity labeling
829 parameters. AIS was defined by endogenous NF186. Biotinylated proteins signal in the AIS
830 and soma was quantified. Images were taken using the same parameter settings in all the
831 conditions of every experiment. Correct mean intensity (CMF) was obtained using mean
832 intensity in target regions extracted by the background of the same image. Labeling
833 efficiency was evaluated by the AIS CMF. Labeling specificity was evaluated by the ratio
834 of AIS CMF/ Soma CMF.
835 smFP-V5 tag knock-in to SCRIB, WDR47 and WDR7 samples at DIV14 were used for
836 polarity analysis. Neurons were infected at DIV0. The AIS was defined by βIV-spectrin
837 labeling. V5 signal was measured in the AIS and proximal dendrites (similar width). A 10-
838 pixel line was drawn along the AIS, or the proximal dendrites to measure the intensity
839 using Fiji-ImageJ software (NIH). Background was extracted and the polarity index was
840 evaluated by the formula AIS/Dendrite ratio= AIS CMF/ Dendrite CMF. At least three
841 independent experiments were performed.
842 DIV14 neurons were used for the integrated AnkG intensity measurement at the AIS.
843 Images were acquired in the focal position for quantification. A 10-pixel line was drawn

844 along the AIS using Fiji-ImageJ software. Integrated AnkG intensity was obtained and
845 normalized against control. Three times independent experiments were performed.
846
847 **Statistical analysis**
848 All statistical analyses were performed in GraphPad Prism 8. The statistical details
849 including the number of experiments, number of cells and statistical tests can be found
850 in figure legends. Statistical analysis was performed by two tailed t-test for two group
851 comparisons and by one-way ANOVA for multiple group comparisons. Graphs are
852 presented as the mean ± SEM. Differences were considered significant when p-values
853 were less than 0.05.
854
855
856 **DATA AVAILABILITY STATEMENT**
857 Raw data of proteome files have been deposited in the ProteomeXchange database under
858 the accession code PXD045921.
859
860

861 **REFERENCES**

862 1. Eichel K, Shen K. The function of the axon initial segment in neuronal polarity.
863 *Developmental biology* **489**, 47-54 (2022).

864

865 2. Kole MH, Stuart GJ. Signal processing in the axon initial segment. *Neuron* **73**, 235-
866 247 (2012).

867

868 3. Grubb MS, Burrone J. Activity-dependent relocation of the axon initial segment
869 fine-tunes neuronal excitability. *Nature* **465**, 1070-1074 (2010).

870

871 4. Kaphzan H, Buffington SA, Jung JI, Rasband MN, Klann E. Alterations in intrinsic
872 membrane properties and the axon initial segment in a mouse model of Angelman
873 syndrome. *The Journal of neuroscience : the official journal of the Society for*
874 *Neuroscience* **31**, 17637-17648 (2011).

875

876 5. Zhang W*, et al.* Formin Activity and mDia1 Contribute to Maintain Axon Initial
877 Segment Composition and Structure. *Molecular neurobiology* **58**, 6153-6169
878 (2021).

879

880 6. Hedstrom KL, Ogawa Y, Rasband MN. AnkyrinG is required for maintenance of the
881 axon initial segment and neuronal polarity. *The Journal of cell biology* **183**, 635-
882 640 (2008).

883

884 7. Sobotzik JM*, et al.* AnkyrinG is required to maintain axo-dendritic polarity in vivo.
885 *Proceedings of the National Academy of Sciences of the United States of America*
886 **106**, 17564-17569 (2009).

887

888 8. Huang CY, Rasband MN. Axon initial segments: structure, function, and disease.
889 *Annals of the New York Academy of Sciences* **1420**, 46-61 (2018).

890

9. Kaphzan H*, et al.* Genetic reduction of the α1 subunit of Na/K-ATPase corrects multiple hippocampal phenotypes in Angelman syndrome. *Cell reports* **4**, 405-412 (2013).

10. Sun X*, et al.* Selective filtering defect at the axon initial segment in Alzheimer's disease mouse models. *Proceedings of the National Academy of Sciences of the United States of America* **111**, 14271-14276 (2014).

11. Leterrier C*, et al.* End-binding proteins EB3 and EB1 link microtubules to ankyrin G in the axon initial segment. *Proceedings of the National Academy of Sciences of the United States of America* **108**, 8826-8831 (2011).

12. Harterink M*, et al.* TRIM46 Organizes Microtubule Fasciculation in the Axon Initial Segment. *The Journal of neuroscience : the official journal of the Society for Neuroscience* **39**, 4864-4873 (2019).

13. van Beuningen SFB*, et al.* TRIM46 Controls Neuronal Polarity and Axon Specification by Driving the Formation of Parallel Microtubule Arrays. *Neuron* **88**, 1208-1226 (2015).

14. Bender KJ, Trussell LO. The physiology of the axon initial segment. *Annual review of neuroscience* **35**, 249-265 (2012).

15. Hedstrom KL*, et al.* Neurofascin assembles a specialized extracellular matrix at the axon initial segment. *The Journal of cell biology* **178**, 875-886 (2007).

16. Leterrier C. The Axon Initial Segment, 50Years Later: A Nexus for Neuronal Organization and Function. *Current topics in membranes* **77**, 185-233 (2016).

17. Hamdan H*, et al.* Mapping axon initial segment structure and function by multiplexed proximity biotinylation. *Nature communications* **11**, 100 (2020).

923 18. Bar DZ, Atkatsh K, Tavarez U, Erdos MR, Gruenbaum Y, Collins FS. Biotinylation by
924 antibody recognition-a method for proximity labeling. *Nature methods* **15**, 127-
925 133 (2018).

926

927 19. Dopie J, Sweredoski MJ, Moradian A, Belmont AS. Tyramide signal amplification
928 mass spectrometry (TSA-MS) ratio identifies nuclear speckle proteins. *The Journal*
929 *of cell biology* **219**, (2020).

930

931 20. Li X*, et al.* Defining Proximity Proteome of Histone Modifications by Antibody-
932 mediated Protein A-APEX2 Labeling. *Genomics, proteomics & bioinformatics* **20**,
933 87-100 (2022).

934

935 21. Chen Y*, et al.* Mapping 3D genome organization relative to nuclear compartments
936 using TSA-Seq as a cytological ruler. *The Journal of cell biology* **217**, 4025-4048
937 (2018).

938

939 22. Hung V*, et al.* Proteomic mapping of the human mitochondrial intermembrane
940 space in live cells via ratiometric APEX tagging. *Molecular cell* **55**, 332-341 (2014).

941

942 23. Loh KH*, et al.* Proteomic Analysis of Unbounded Cellular Compartments: Synaptic
943 Clefts. *Cell* **166**, 1295-1307.e1221 (2016).

944

945 24. Fréal A*, et al.* Feedback-Driven Assembly of the Axon Initial Segment. *Neuron* **104**,
946 305-321.e308 (2019).

947

948 25. Torii T*, et al.* NuMA1 promotes axon initial segment assembly through inhibition
949 of endocytosis. *The Journal of cell biology* **219**, (2020).

950

951 26. Ke M*, et al.* Spatiotemporal profiling of cytosolic signaling complexes in living cells
952 by selective proximity proteomics. *Nature communications* **12**, 71 (2021).

953

954 27. Zhou Y*, et al.* Expanding APEX2 Substrates for Proximity-Dependent Labeling of
955 Nucleic Acids and Proteins in Living Cells. *Angewandte Chemie (International ed in*
956 *English)* **58**, 11763-11767 (2019).

957

958 28. Lind D, Franken S, Kappler J, Jankowski J, Schilling K. Characterization of the
959 neuronal marker NeuN as a multiply phosphorylated antigen with discrete
960 subcellular localization. *Journal of neuroscience research* **79**, 295-302 (2005).

961

962 29. Wolf HK*, et al.* NeuN: a useful neuronal marker for diagnostic histopathology. *The*
963 *journal of histochemistry and cytochemistry : official journal of the Histochemistry*
964 *Society* **44**, 1167-1171 (1996).

965

966 30. Dehmelt L, Halpain S. The MAP2/Tau family of microtubule-associated proteins.
967 *Genome biology* **6**, 204 (2005).

968

969 31. Thompson A*, et al.* Tandem mass tags: a novel quantification strategy for
970 comparative analysis of complex protein mixtures by MS/MS. *Analytical chemistry*
971 **75**, 1895-1904 (2003).

972

973 32. Eichel K*, et al.* Endocytosis in the axon initial segment maintains neuronal polarity.
974 *Nature* **609**, 128-135 (2022).

975

976 33. Jones SL, Korobova F, Svitkina T. Axon initial segment cytoskeleton comprises a
977 multiprotein submembranous coat containing sparse actin filaments. *The Journal*
978 *of cell biology* **205**, 67-81 (2014).

979

980 34. Bas Orth C, Schultz C, Müller CM, Frotscher M, Deller T. Loss of the cisternal
981 organelle in the axon initial segment of cortical neurons in synaptopodin-deficient
982 mice. *The Journal of comparative neurology* **504**, 441-449 (2007).

983

984 35. Ogawa Y, Horresh I, Trimmer JS, Bredt DS, Peles E, Rasband MN. Postsynaptic
985 density-93 clusters Kv1 channels at axon initial segments independently of Caspr2.

986 *The Journal of neuroscience : the official journal of the Society for Neuroscience* **28**,
987 5731-5739 (2008).

988

989 36. Merkulova M, Păunescu TG, Azroyan A, Marshansky V, Breton S, Brown D.
990 Mapping the H(+) (V)-ATPase interactome: identification of proteins involved in
991 trafficking, folding, assembly and phosphorylation. *Scientific reports* **5**, 14827
992 (2015).

993

994 37. Crummy E, Mani M, Thellman JC, Martin TFJ. The priming factor CAPS1 regulates
995 dense-core vesicle acidification by interacting with rabconnectin3β/WDR7 in
996 neuroendocrine cells. *The Journal of biological chemistry* **294**, 9402-9415 (2019).

997

998 38. Gowrisankaran S, Milosevic I. Regulation of synaptic vesicle acidification at the
999 neuronal synapse. *IUBMB life* **72**, 568-576 (2020).

1000

1001 39. Chen Y*, et al.* Wdr47 Controls Neuronal Polarization through the Camsap Family
1002 Microtubule Minus-End-Binding Proteins. *Cell reports* **31**, 107526 (2020).

1003

1004 40. Buijs RR*, et al.* WDR47 protects neuronal microtubule minus ends from katanin-
1005 mediated severing. *Cell reports* **36**, 109371 (2021).

1006

1007 41. Moreau MM*, et al.* The planar polarity protein Scribble1 is essential for neuronal
1008 plasticity and brain function. *The Journal of neuroscience : the official journal of*
1009 *the Society for Neuroscience* **30**, 9738-9752 (2010).

1010

1011 42. Roche JP, Packard MC, Moeckel-Cole S, Budnik V. Regulation of synaptic plasticity
1012 and synaptic vesicle dynamics by the PDZ protein Scribble. *The Journal of*
1013 *neuroscience : the official journal of the Society for Neuroscience* **22**, 6471-6479
1014 (2002).

1015

1016 43. Szczurkowska J*, et al.* A Localized Scaffold for cGMP Increase Is Required for Apical
1017 Dendrite Development. *Cell reports* **31**, 107519 (2020).

1018

1019 44. Gao Y*, et al.* Plug-and-Play Protein Modification Using Homology-Independent
1020 Universal Genome Engineering. *Neuron* **103**, 583-597.e588 (2019).

1021

1022 45. Garrido JJ*, et al.* A targeting motif involved in sodium channel clustering at the
1023 axonal initial segment. *Science (New York, NY)* **300**, 2091-2094 (2003).

1024

1025 46. Winckler B, Forscher P, Mellman I. A diffusion barrier maintains distribution of
1026 membrane proteins in polarized neurons. *Nature* **397**, 698-701 (1999).

1027

1028 47. Leterrier C, Potier J, Caillol G, Debarnot C, Rueda Boroni F, Dargent B. Nanoscale
1029 Architecture of the Axon Initial Segment Reveals an Organized and Robust Scaffold.
1030 *Cell reports* **13**, 2781-2793 (2015).

1031

1032 48. Xu K, Zhong G, Zhuang X. Actin, spectrin, and associated proteins form a periodic
1033 cytoskeletal structure in axons. *Science (New York, NY)* **339**, 452-456 (2013).

1034

1035 49. Zhang W, Bonadiman A, Ciorraga M, Benitez MJ, Garrido JJ. P2Y1 Purinergic
1036 Receptor Modulate Axon Initial Segment Initial Development. *Frontiers in cellular*
1037 *neuroscience* **13**, 152 (2019).

1038

1039 50. Ezan J*, et al.* Early loss of Scribble affects cortical development, interhemispheric
1040 connectivity and psychomotor activity. *Scientific reports* **11**, 9106 (2021).

1041

1042 51. Wells C*, et al.* First fetal case of the 8q24.3 contiguous genes syndrome. *American*
1043 *journal of medical genetics Part A* **170a**, 239-242 (2016).

1044

1045 52. Lei Y*, et al.* Mutations in planar cell polarity gene SCRIB are associated with spina
1046 bifida. *PloS one* **8**, e69262 (2013).

1047

1048 53. Robinson A*, et al.* Mutations in the planar cell polarity genes CELSR1 and SCRIB are
1049 associated with the severe neural tube defect craniorachischisis. *Human mutation*
1050 **33**, 440-447 (2012).

54. Frankenfield AM, Fernandopulle MS, Hasan S, Ward ME, Hao L. Development and Comparative Evaluation of Endolysosomal Proximity Labeling-Based Proteomic Methods in Human iPSC-Derived Neurons. *Analytical chemistry* **92**, 15437-15444 (2020).

55. Aguilan JT, Kulej K, Sidoli S. Guide for protein fold change and p-value calculation for non-experts in proteomics. *Molecular omics* **16**, 573-582 (2020).

56. Ogawa Y, Rasband MN. Endogenously expressed Ranbp2 is not at the axon initial segment. *Journal of cell science* **134**, (2021).

ACKNOWLEDGMENTS

We thank Y. Li, G. Wang, F. Yuan and Y. Chen for helpful discussions. This work was supported by the Ministry of Science and Technology (2018YFA0507600, 2017YFA0503600), the National Natural Science Foundation of China (32088101, 21727806), and a grant from the National Institutes of Neurological Disorders and Stroke (NS122073 to M.N.R.). P.Z. is sponsored by Bayer Investigator Award. W.Z. was supported in part by the Postdoctoral Fellowship of Peking-Tsinghua Center for Life Sciences. We thank Ms. W. Zhou from the Analytical Instrumentation Center in Peking University for assistance with MS sample identification.

AUTHOR CONTRIBUTIONS

W.Z., P.Z. and M.N.R. conceived the project. W.Z., P.Z. and M.N.R. designed experiments. W.Z., Y.F., L.P., Y.O., X.D., A.R., X.Z., and M.S. performed experiments. W.Z. and P.Z. analyzed the data and wrote the paper with input from all authors. W.Z., P.Z. and M.N.R. revised the paper.

COMPETING INTERESTS

The authors declare no competing interests.

FIGURES

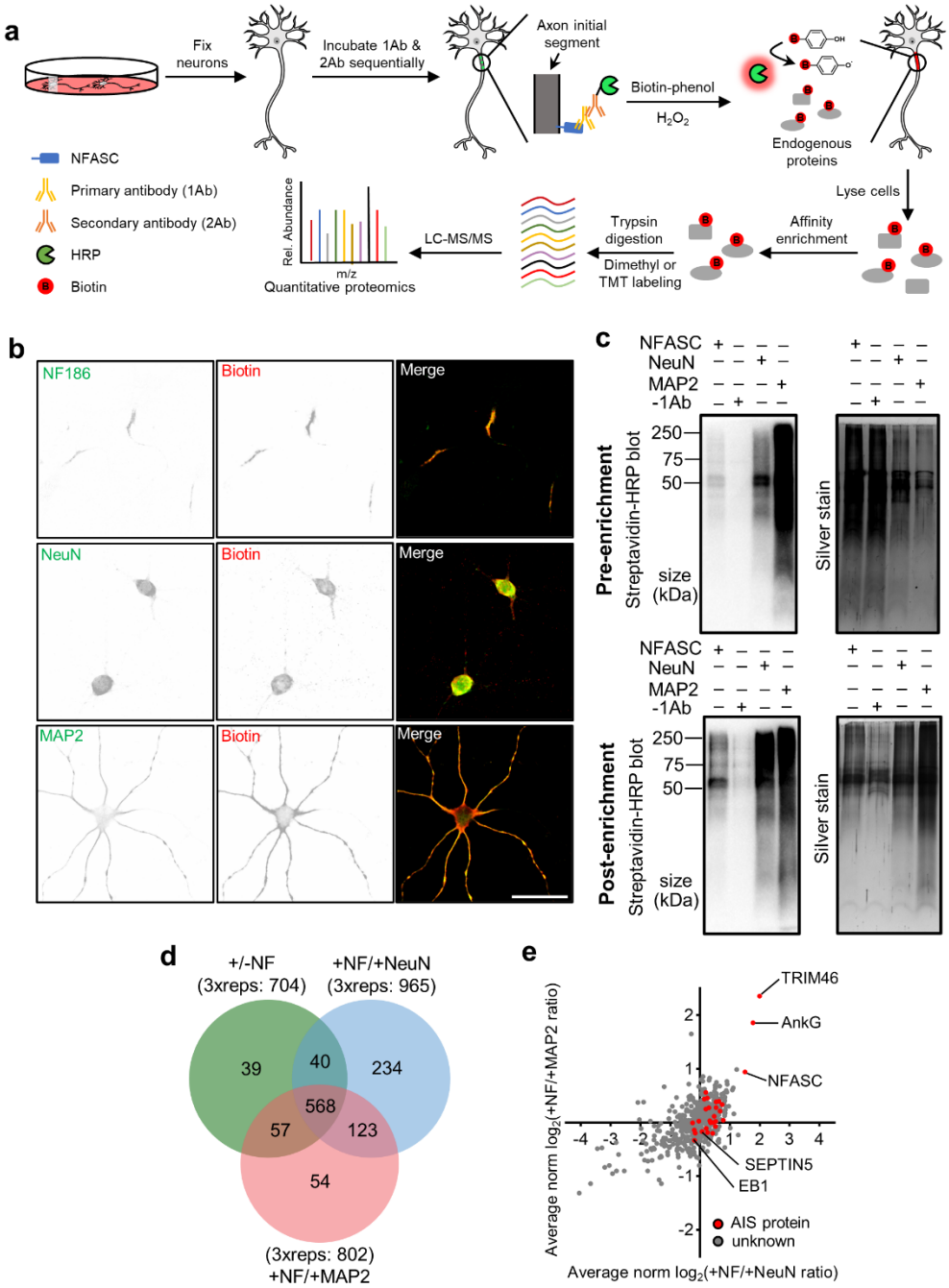

Figure 1. Immunoproximity labeling of AIS

a, Experimental scheme of IPL-AIS method. HRP is directed to the axon initial segment in fixed cortical neurons through the specific binding of anti-NFASC antibodies (1Ab) and HRP conjugated secondary antibodies (2Ab). HRP-mediated proximity biotinylation is

1088 mediated by the addition of biotin-phenol substrates and hydrogen peroxide. Biotinylated
1089 proteins are enriched via affinity purification, digested with trypsin, and identified via LC-
1090 MS/MS analysis.
1091 **b**, Biotinylated proteins colocalize with endogenous protein signals in the axon initial
1092 segment, soma and somatodendrites. The proximity labeling was directed by anti-NFASC,
1093 anti-NeuN and anti-MAP2 antibodies individually in DIV14 cortical neurons with one
1094 minute of reaction time. Scale bar= 50 µm.
1095 **c**, Streptavidin blots and silver staining of DIV12 cortical neuron lysates (pre-enrichment)
1096 or streptavidin bead eluates (post-enrichment) in conditions of anti-NFASC, no primary
1097 antibody (-1Ab), anti-NeuN and anti-MAP2 targeted proximity labeling. Samples of anti-
1098 NFASC, -1Ab, anti-NeuN and anti-MAP2 were loaded as the ratio of 4:4:2:1.
1099 **d**, Venn diagrams showing 568 overlapping biotinylated proteins from +NFASC/+NeuN,
1100 +NFASC/+MAP2 and filtered +/-NFASC datasheet. Three independent dimethyl proteome
1101 replicates were performed at DIV14 for each condition.
1102 **e**, Scatterplot showing the enrichment of anti-NFASC captured biotinylated proteins over
1103 soma (x-axis) and somatodendrites (y-axis) intensity in the reference of average
1104 normalized $\log_2$(H/L ratios). Red dots indicate reported AIS components and gray dots are
1105 proteins having no AIS information.

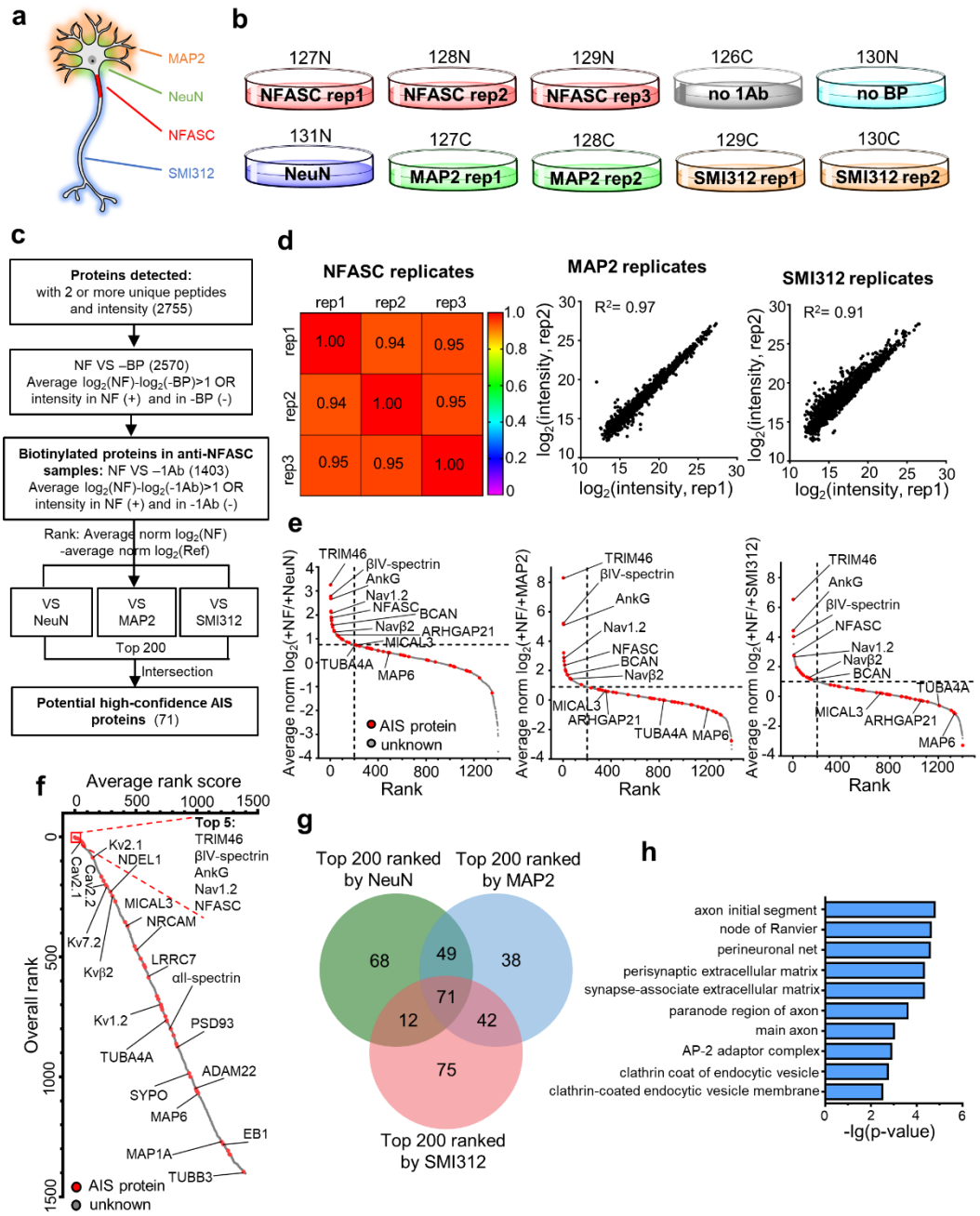

Figure 2. The axon initial segment proteome at DIV14.

a, Schematic of neurons biotinylated at the axon initial segment by targeting NFASC (red), soma by targeting NeuN (green), somatodendrites by targeting MAP2 (orange), and axon by targeting phosphorylated neurofilaments using SMI312 antibody (blue).

b, Design of 10-plex TMT for AIS quantitative proteomic experiments. Samples were

1111 collected from at least three independent primary neuron cultures for each condition.
1112 TMT tags were labelled on the dishes.
1113 **c**, Workflow for AIS proteome analysis.
1114 **d**, Correlation analysis of biological replicates showing high reproducibility. Pearson
1115 correlation was applied to parallel analysis of 2377, 2691 and 2498 common elements in
1116 anti-NFASC, anti-MAP2 and anti-SMI312 replicates, respectively.
1117 **e**, Ranking of 1403 biotinylated proteins based on their averaged MS intensity ratios. Red
1118 dots indicate previously reported AIS components and gray dots are proteins having no
1119 AIS information.
1120 **f**, Overall rank plot integrating three reference proteomes (e) listing potential AIS enriched
1121 proteins in the top positions. Proteins are sorted by average rank scores from
1122 +NFASC/+NeuN, +NFASC/+MAP2 and +NFASC/+SMI312 experiments. Red dots indicate
1123 reported AIS components and gray dots are proteins having no AIS information. Some AIS
1124 proteins are labelled.
1125 **g**, Venn diagrams showing 71 high-confidence AIS proteins from the top 200 candidates
1126 from +NFASC/+NeuN, +NFASC/+MAP2 and +NFASC/+SMI312 proteomes.
1127 **h**, Top 10 cellular compartment terms. 71 high-confidence AIS candidates were applied to
1128 Gene Ontology cellular compartment analysis. A total of 2744 valid proteins in this TMT
1129 were used as a reference (2755 proteins identified and 2744 valid data in Gene Ontology).

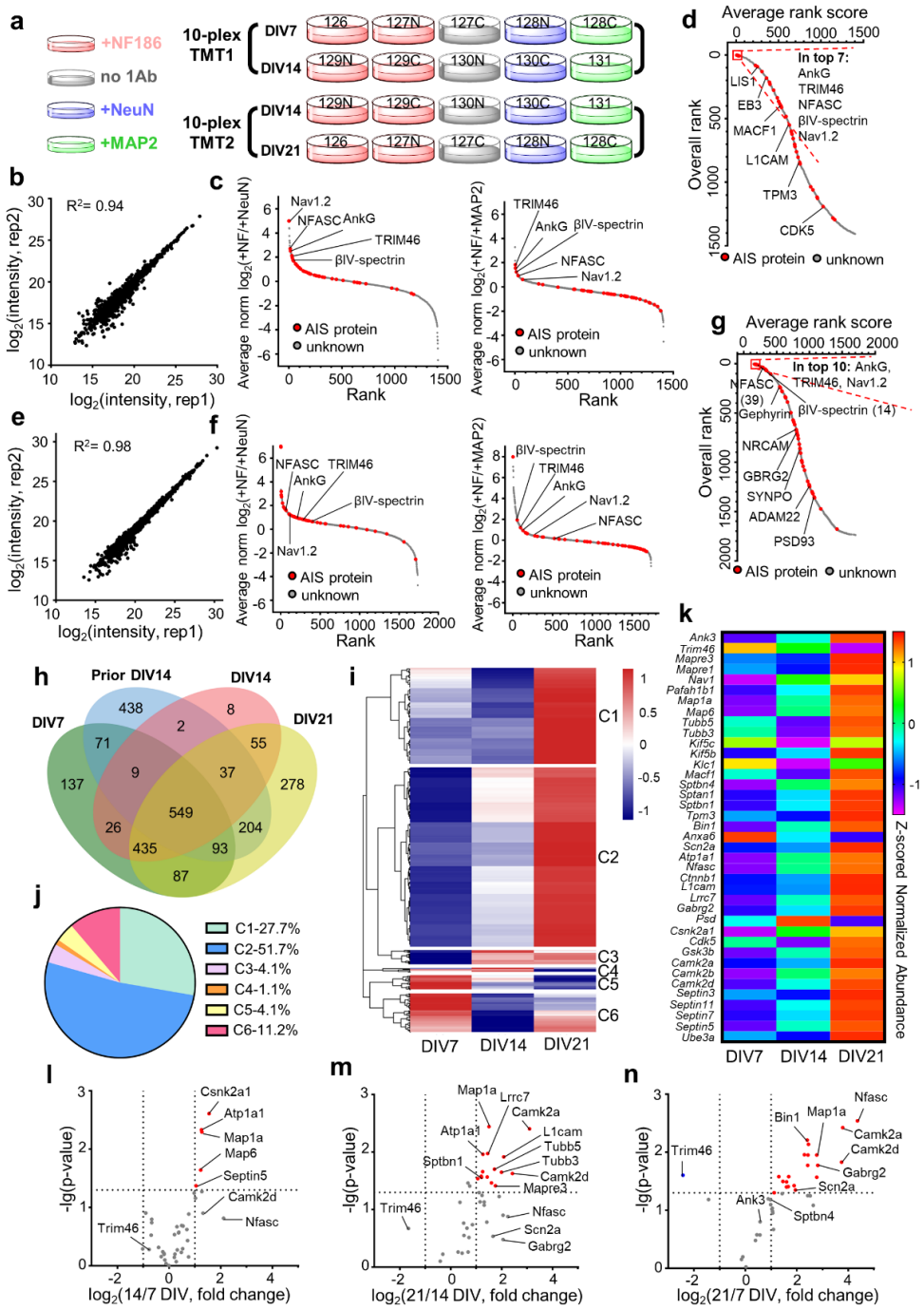

Figure 3. The axon initial segment proteome across development.

a, Experimental design to evaluate the AIS proteome during development using two parallel 10-plex TMT: DIV7 for early AIS, DIV14 for mature AIS and DIV21 for mature AIS. **b**, Pearson correlation showing high reproducibility in anti-NFASC targeted AIS proximity

1134 labeling for DIV7 cortical neurons (1532 common elements from 2 replicates).

1135 **c**, Ranking DIV7 AIS biotinylated 1407 proteins according to their averaged MS intensity
1136 ratios (+NFASC/+NeuN and +NFASC/+MAP2).

1137 **d**, DIV7 overall rank plot listing potential AIS proteins. Proteins are sorted by the average
1138 rank scores from +NFASC/+NeuN and +NFASC/+MAP2 experiments from (c). Some known
1139 AIS proteins are labelled in the graph. Red dots indicate reported AIS components and
1140 gray dots are proteins having no AIS information.

1141 **e**, Pearson correlation showing high reproducibility in anti-NFASC targeted AIS proximity
1142 labeling for DIV21 cortical neurons (1859 common elements from 2 replicates).

1143 **f**, Ranking DIV21 AIS biotinylated 1738 proteins according to their averaged MS intensity
1144 ratios (+NFASC/+NeuN and +NFASC/+MAP2).

1145 **g**, DIV21 overall rank plot listing potential AIS proteins. Proteins are sorted by the average
1146 rank scores from +NFASC/+NeuN and +NFASC/+MAP2 experiments from (f). Some known
1147 AIS proteins are labelled in the graph. Red dots indicate reported AIS components and
1148 gray dots are proteins having no AIS information.

1149 **h**, Venn diagrams showing 549 common AIS candidates at DIV7, 14 and 21. The prior AIS
1150 proteome at DIV14 was also included in this analysis.

1151 **i**, Six clusters with distinct protein expression profiles were generated by pheatmap
1152 analysis in R package along neuronal development.

1153 **j**, The percentage of protein numbers in each cluster of the 534 analyzed proteins.

1154 **k**, AIS protein expression patterns along neuronal development. Proteins are represented
1155 by their gene names.

1156 **l-n**, Volcano plots showing fold changes in AIS proteins between DIV7 and 14 (l), DIV 14
1157 and 21 (m) or DIV7 and 21 (n). Red and blue points represent AIS proteins with significant
1158 up-regulation and down-regulation respectively. Proteins are represented by their gene
1159 names. Horizontal dashed lines indicate p= 0.05. Vertical dashed lines indicate the cutoff
1160 of $\log_2$(fold change) = ±1.

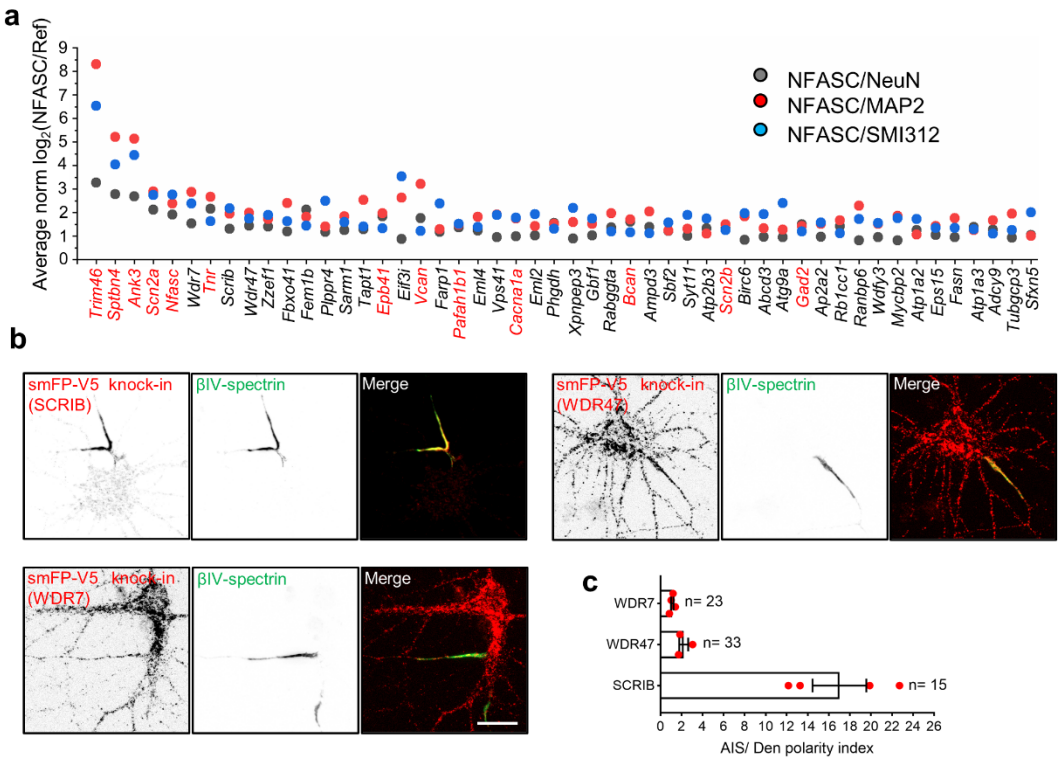

Figure 4. Screening AIS candidates by tagging endogenous genes.

a, Top 50 ranked AIS candidates at DIV14. The fold change of proteins intensity in the AIS compared with soma, somatodendrites and the axon. Previously reported AIS proteins are shown in red, and the rest are shown in black. Proteins are represented by their gene names.

b, Representative images of smFP-V5 tag knock-in neurons for SCRIB, WDR47, and WDR7. Neurons were infected with two AAVs, one is for Cas9 expression and another for gRNA and donor expression for homology-independent knock-in at DIV0. Samples were fixed at DIV14 and labelled with βIV-spectrin (green, AIS) and V5 tag (red, targeted proteins). Scale bar= 20 µm.

c, Quantification of V5 tag mean intensity in the AIS versus in proximal dendrites from knock-in samples. Four independent experiments were performed for WDR7 (n= 23 neurons) and SCRIB (n= 15 neurons). Three independent experiments were performed for

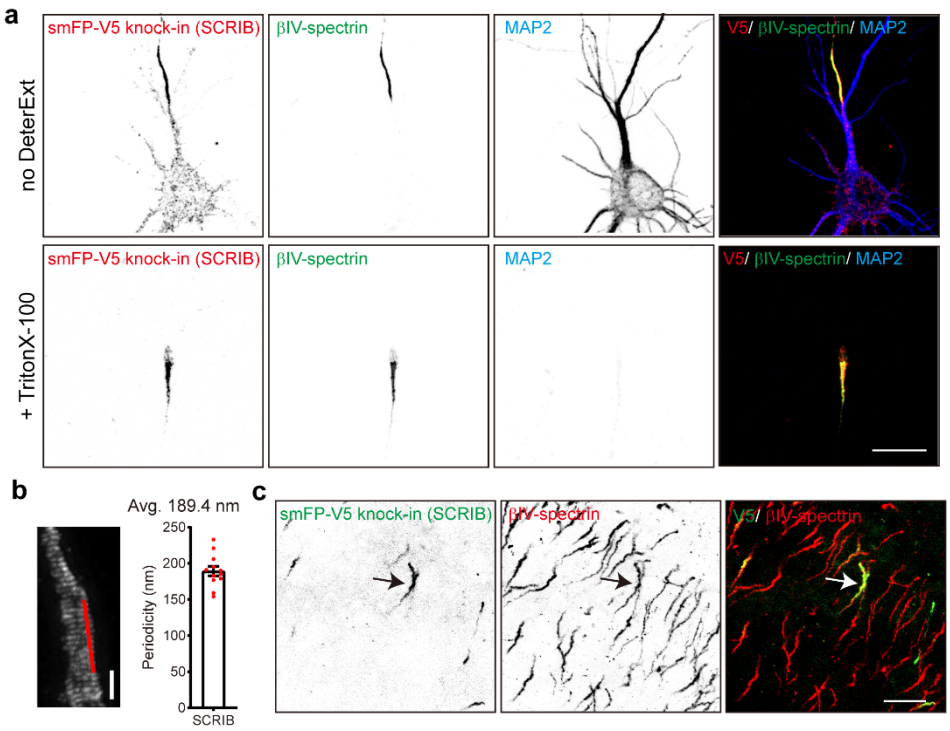

WDR47 (n= 33 neurons). Data are shown as mean ± SEM.

Figure 5. Validation of SCRIB enrichment at the AIS *in vitro* and *in vivo* by knock-in.

a, Representative images of smFP-V5 tag knock-in to endogenous SCRIB. Live neurons were treated with or without 0.5% TritonX-100. Neurons were infected at DIV0. After 14 days, samples were immunolabeled for the V5 tag (red, endogenous SCRIB), βIV-spectrin (green, AIS), and MAP2 (blue, somatodendrites). Scale bar= 20 µm.

b, A representative STED image of smFP-V5 tagged SCRIB. Knock-in neurons were fixed at DIV16, and stained with V5 tag antibody. Regions indicated by red lines were used to generate the intensity profiles, and the average periodicities were calculated. Column is mean ± SEM. Scale bar= 1 µm.

c, Representative image of smFP-V5 tagged SCRIB in the cortex. P0 Cas9 pups were intraventricularly injected with mouse specific *Scrib* gRNA and donor AAV and sacrificed at postnatal day 23 (P23). Samples were stained for the V5 tag (green, endogenous SCRIB) and βIV-spectrin (red, AIS). Scale bar = 20 µm.

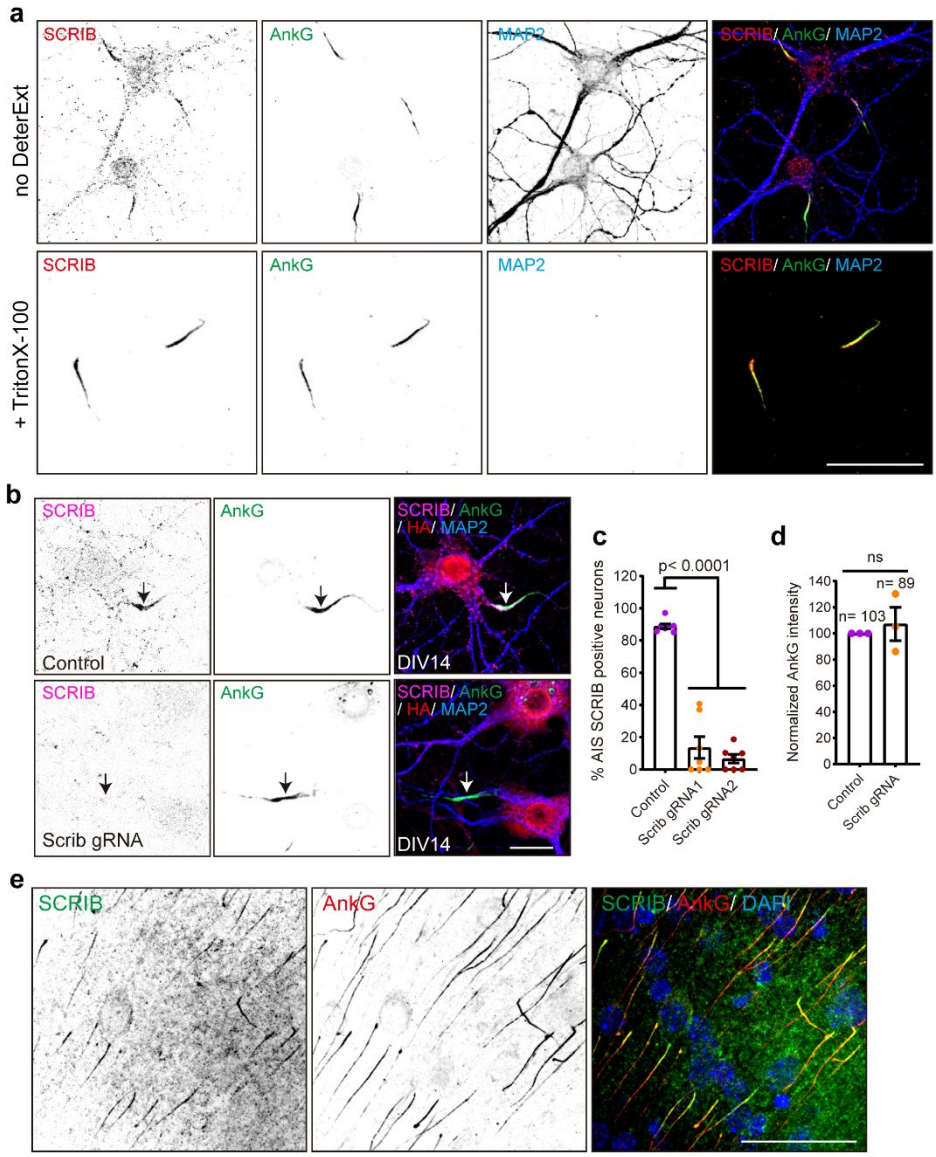

1190

1191

1192 **Figure 6. Validation of SCRIB enrichment at the AIS *in vitro* and *in vivo* by**

1193 **immunostaining.**

1194 **a**, Representative images of DIV14 neurons treated with or without 0.5% TritonX-100

1195 extraction prior to fixation. Fixed hippocampal neurons were stained with SCRIB (red),

1196 AnkG (green, AIS), and MAP2 (blue, somatodendrites). Scale bar = 50 µm.

1197 **b**, Representative images of SCRIB knock-out using the CRISPR-Cas9 system. Hippocampal

1198 neurons were infected at DIV0 with AAV to express *Scrib* triple gRNA or template plasmids;

1199 both also harbor an HA expression cassette. Neurons were fixed at DIV14 and stained for
1200 SCRIB (magenta), AnkG (green), HA (red), and MAP2 (blue). Arrows indicate the AIS. Scale
1201 bar = 20 µm.
1202 **c**, Quantification of the percentage of AIS SCRIB positive neurons. Seven independent
1203 experiments were performed using two different *Scrib* triple gRNA to disrupt *Scrib*
1204 expression. 30~50 transfected neurons in each condition for each experiment were
1205 analyzed. Data are mean ± SEM. One-way ANOVA, $p<0.0001$.
1206 **d**, Comparison of integrated AnkG intensity in the AIS 14 days after transduction with AAV
1207 to disrupt *Scrib* expression. Three independent experiments were performed. Data are
1208 mean ± SEM. Unpaired t test followed by Welch's correction; ns, not significant.
1209 **e**, Coronal cortical sections from P7 mice were stained for SCRIB (green), AnkG (red) and
1210 nuclei (DAPI, blue). Scale bar= 50 µm.
1211

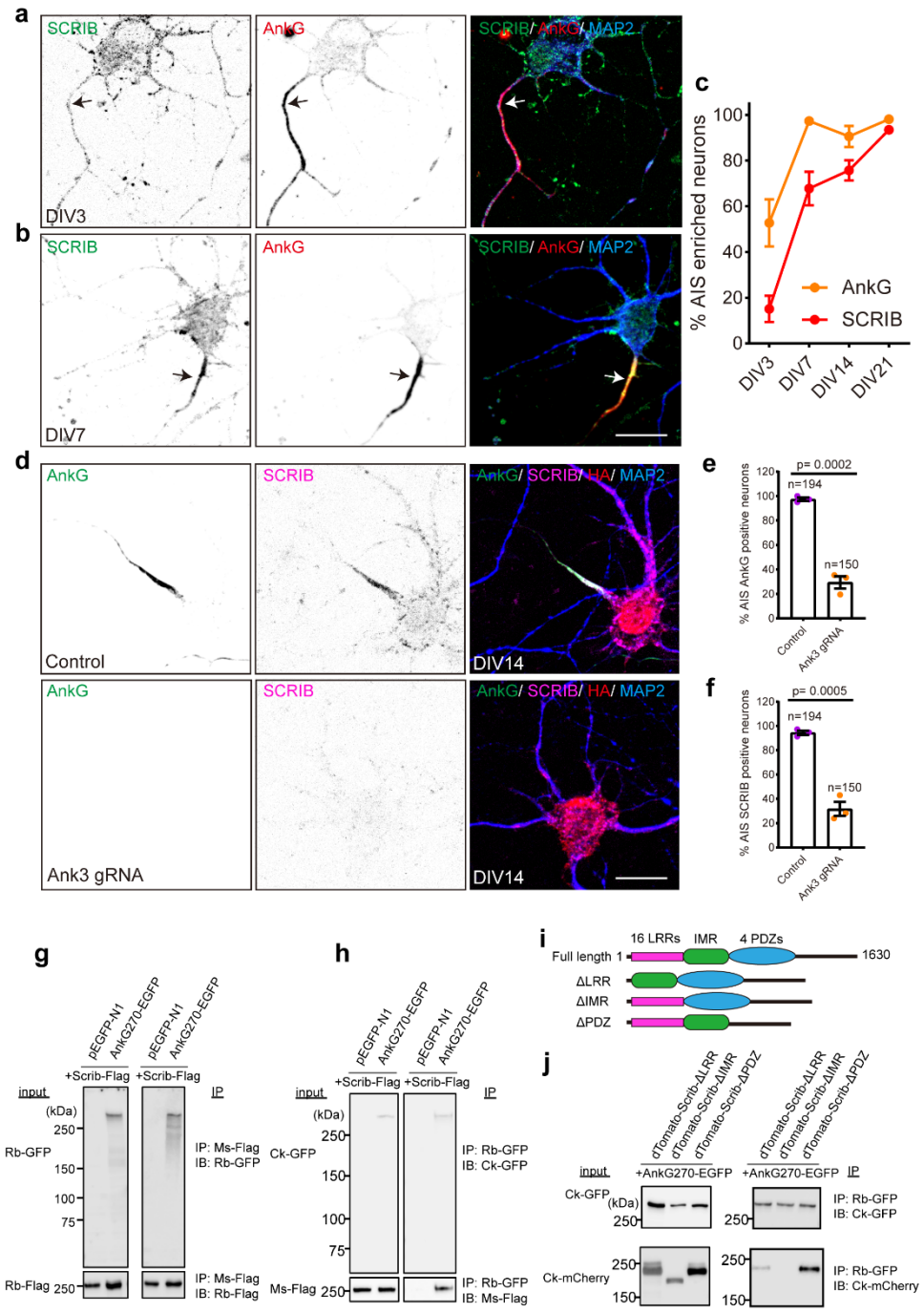

Figure 7. AnkG is required for SCRIB enrichment at the AIS.

a-b, Representative images of DIV3 (a) and DIV7 (b) hippocampal neurons stained for SCRIB (green), AnkG (red), and MAP2 (blue). Arrows indicate the proximal axon (a) and AIS (b). Scale bar= 20 µm.

1217 **c**, Quantification of the percentage of neurons with AIS SCRIB and AnkG at DIV3, 7, 14 and
1218 21. Four independent experiments were performed at each time point. Data are mean ±
1219 SEM.
1220 **d**, Representative images of AnkG knock-out using the CRISPR-Cas9 system. DIV0
1221 hippocampal neurons were transduced with *Ank3* triple gRNA or template plasmids; the
1222 plasmids also harbor an HA expression cassette. Neurons were fixed at DIV14 and stained
1223 for SCRIB (magenta), AnkG (green), HA (red), and MAP2 (blue). Scale bar= 20 µm.
1224 **e-f**, Quantification of the percentage of neurons with AIS AnkG (e) and SCRIB (f) after loss
1225 transduction with AAV to disrupt AnkG expression. Three independent experiments were
1226 performed with the number of neurons analyzed indicated on the figure. Data are mean
1227 ± SEM. Unpaired t test, p= 0.0002 (e) and p= 0.0005 (f).
1228 **g-h**, Co-immunoprecipitation of Scrib-Flag with AnkG270-EGFP. Scrib-Flag and AnkG270-
1229 EGFP or pEGFPN1 were co-transfected in HEK293T cells and immunoprecipitated by Flag
1230 antibody (g) or GFP antibody (h). IP, immunoprecipitation. IB, immunoblotting. Rb-GFP,
1231 rabbit anti-GFP. Rb-Flag, rabbit anti-Flag. Ms-Flag, mouse anti-Flag. Ck-GFP, chicken anti-
1232 GFP.
1233 **i**, Illustration of the full length and SCRIB truncation constructs used.
1234 **j**, Co-immunoprecipitation of truncated SCRIB with AnkG270. IP, immunoprecipitation. IB,
1235 immunoblotting. Ck-GFP, chicken anti-GFP. Ck-mCherry, chicken anti-mCherry. Rb-GFP,
1236 rabbit anti-GFP.
1237

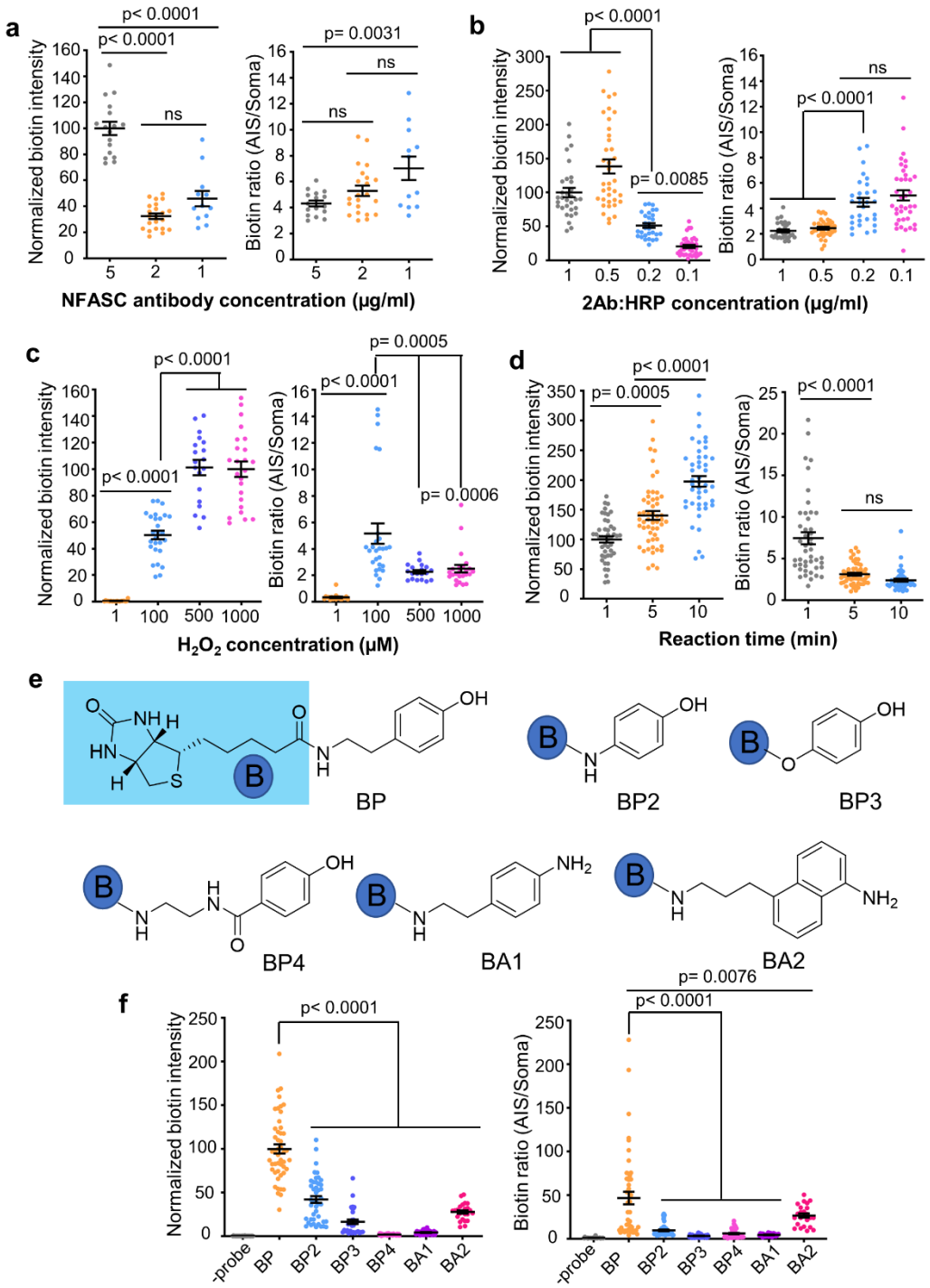

Supplementary Figure 1. Optimization of anti-NFASC directed proximity labeling. **a-f**, Anti-NFASC antibody directed proximity labeling parameters were tested in DIV10-14 fixed cortical neurons. Tested parameters are as follows: first antibody (1Ab, a), HRP

1241 conjugated second antibody (2Ab, b) and H_2O_2 concentration (c), reaction duration (d) and
1242 reaction substrates (f). The stock concentration of 1Ab and 2Ab is 1 mg/ml. (e) Chemical
1243 probes tested in this study. The labeling efficiency was evaluated by the mean intensity of
1244 biotinylated proteins signal in the AIS. The labeling specificity was evaluated by the ratio
1245 of biotinylated protein signal in the AIS against that in the soma. Each point represents
1246 one neuron. Graphs are presented as mean ± SEM, one-way ANOVA, p-values are
1247 indicated on the figure and ns, not significant.
1248

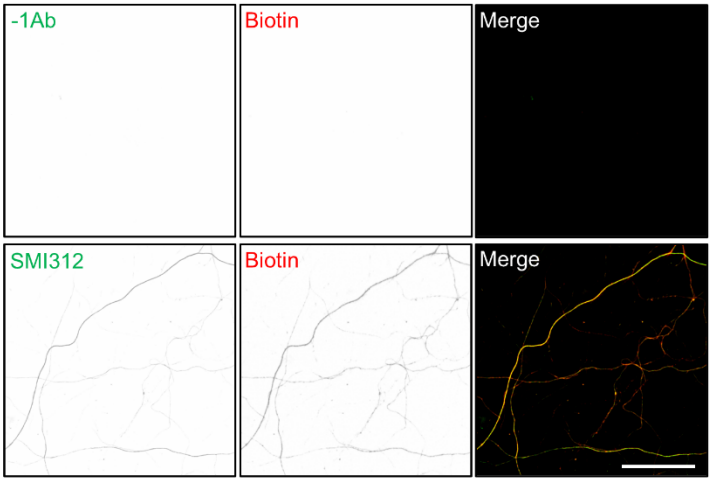

1249

1250 **Supplementary Figure 2. SMI312 directed proximity labeling.** Fixed DIV14 cortical
1251 neurons were processed for proximity labeling with or without SMI312 antibody.
1252 Biotinylated proteins are in red, endogenous proteins labelled by SMI312 is in green. Scale
1253 bar = 50 µm.
1254

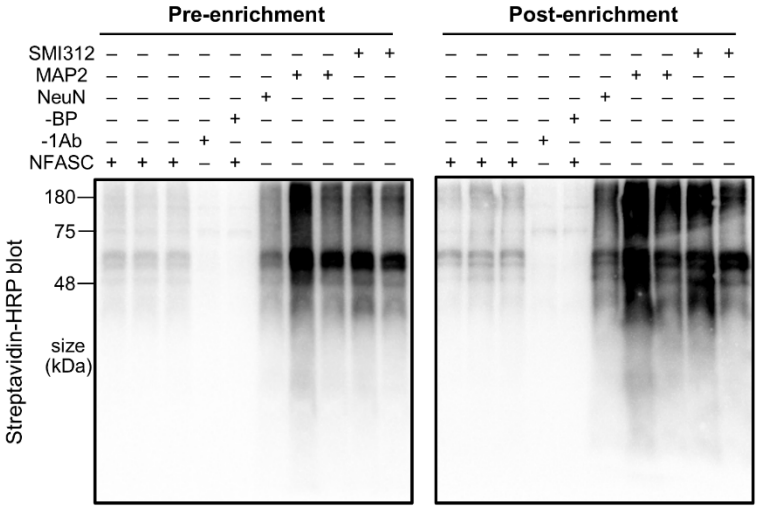

1255 **Supplementary Figure 3. Proximity labeling and enrichment in DIV14 TMT experiments.**
1256 Streptavidin blots of DIV14 cortical neuron lysates (pre-enrichment) or streptavidin bead
1257 eluate (post-enrichment) from samples of anti-NFASC, NeuN, MAP2, SMI312 and no
1258 primary antibody (-1Ab) or substrate BP (-BP). Samples of anti-NFASC, -1Ab, -BP, anti-
1259 NeuN, anti-MAP2 and anti-SMI312 were loaded as the ratio of 3: 3: 3: 1: 1: 1, respectively.

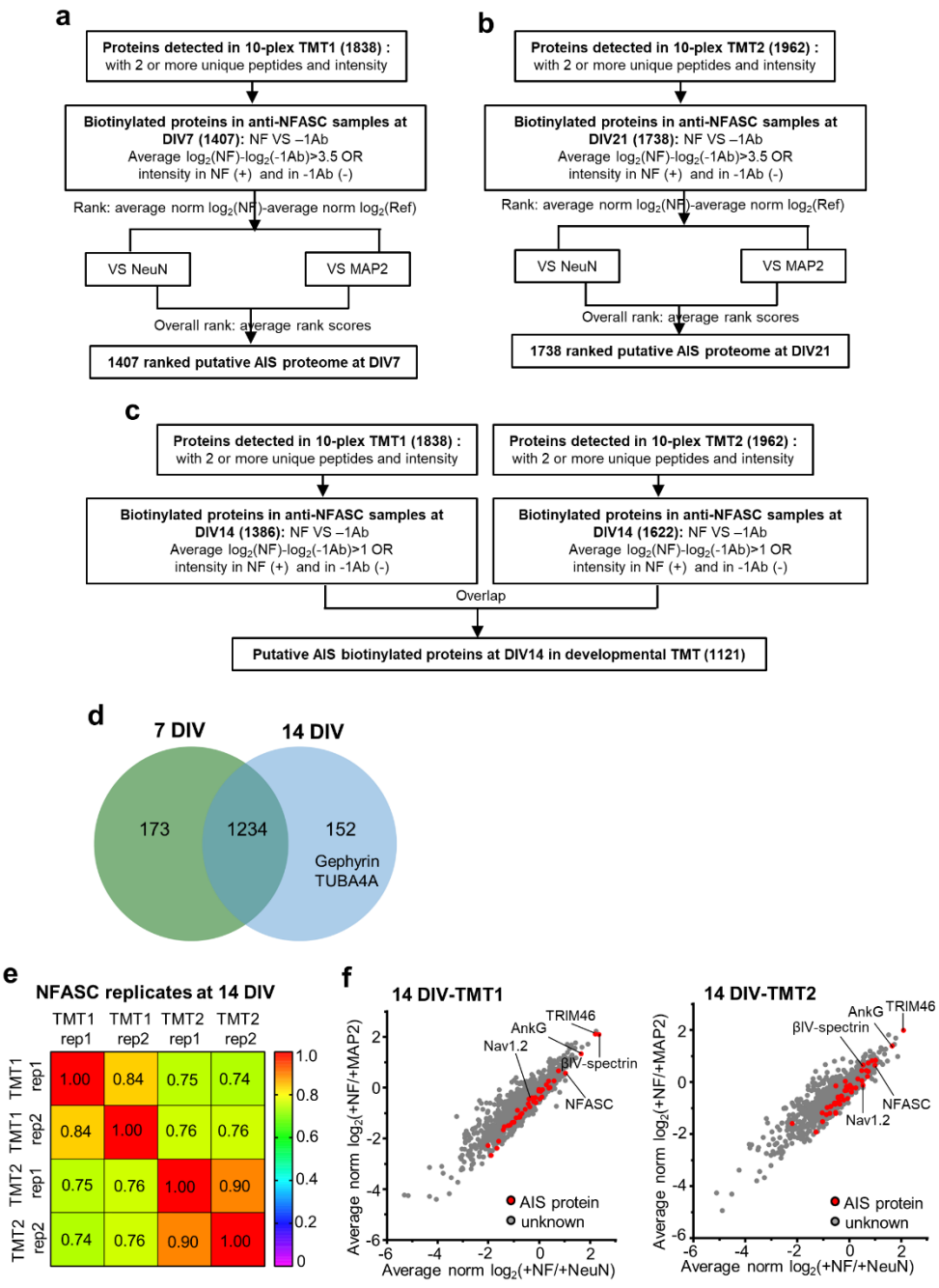

Supplementary Figure 4. The AIS developmental proteome.

a-c, Workflow for DIV7 (a), 21 (b) and 14 (c) biotinylated protein analysis in anti-NFASC samples.

d, Venn diagram of anti-NFASC targeted biotinylated proteins between DIV7 and 14 in 10-

1264 plex TMT1.

1265 **e-f**, Analysis of DIV14 anti-NFASC targeted biotinylated proteins from two parallel TMT
1266 experiments. (e) Correlation analysis of biological replicates showing high reproducibility
1267 in anti-NFASC directed AIS proximity labeling from two 10-plex TMT experiments. (f)
1268 Scatterplot showing the enrichment of anti-NFASC targeted biotinylated proteins against
1269 soma (x-axis) and somatodendrites (y-axis). Red dots indicate reported AIS components
1270 and gray dots are proteins having no AIS information.

1271

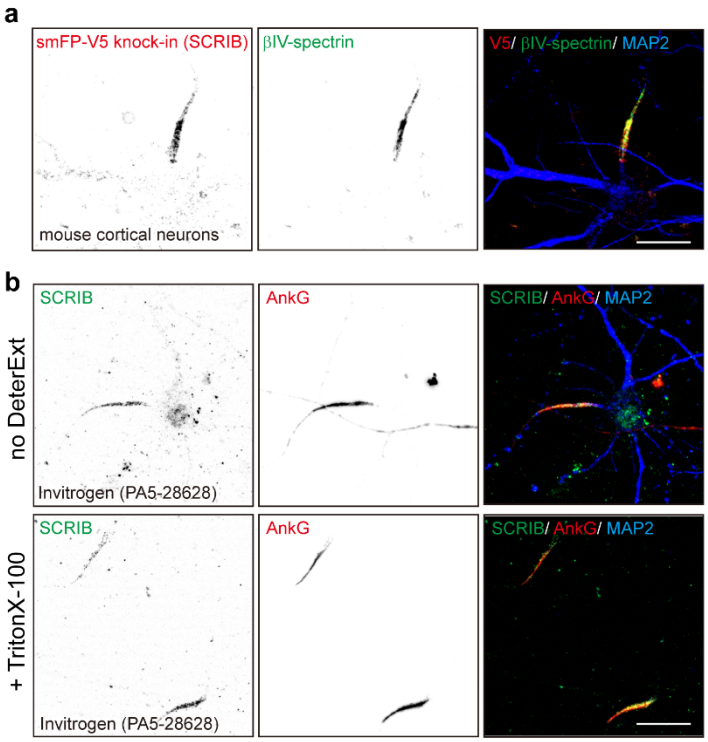

Supplementary Figure 5. SCRIB localizes at the AIS.

a, Representative image of smFP-V5-tagged SCRIB in Cas9 transgenic mouse neurons. Cortical neurons were infected at DIV0 with gRNA and donor AAV and fixed at DIV10. Samples were stained for the V5 tag (red, endogenous SCRIB), βIV-spectrin (green, AIS), and MAP2 (blue, somatodendrites). Scale bar = 20 µm.

b, Representative images of DIV14 rat neurons stained with the Invitrogen SCRIB antibody targeting amino acids 1568-1630. Hippocampal neurons were treated with or without 0.5% TritonX-100 before fixation and stained for SCRIB (green), AnkG (red, AIS), and MAP2 (blue, somatodendrites). Scale bar = 20 µm.